ELECTRONIC SUPPORTING INFORMATION

How to tune luminescent Cu(I) complexes with strong donor carbenes towards TADF?

Jasper Guhl,[†[a]] Dragana Sretenović,[†[b]] Philipp Schmeinck,[[c]] Suren Felekyan,[[b]] Ralf Kühnemuth,[[b]] Christian Ganter,[[c]] Claus A. M. Seidel,[*[b]] Christel M. Marian,[*[a]] and Markus Suta[*[c]]

[†] These authors contributed equally.

[a] J. Guhl, Prof. Dr. C. M. Marian
Institute of Theoretical and Computational Chemistry
Heinrich Heine University Düsseldorf
Universitätsstr. 1, 40225 Düsseldorf, Germany
E-mail: christel.marian@hhu.de

[b] D. Sretenović, Dr. S. Felekyan, Dr. R. Kühnemuth, Prof. Dr. C. A. M. Seidel
Institute of Physical Chemistry
Heinrich Heine University Düsseldorf
Universitätsstr. 1, 40225 Düsseldorf, Germany
E-mail: cseidel@hhu.de

[c] P. Schmeinck, Prof. Dr. C. Ganter, Jun.-Prof. Dr. M. Suta
Institute of Inorganic and Structural Chemistry
Heinrich Heine University Düsseldorf
Universitätsstr. 1, 40225 Düsseldorf, Germany
E-mail: markus.suta@hhu.de

Table of Contents

1. Spectral Properties

1.1. Correction of absorption spectra

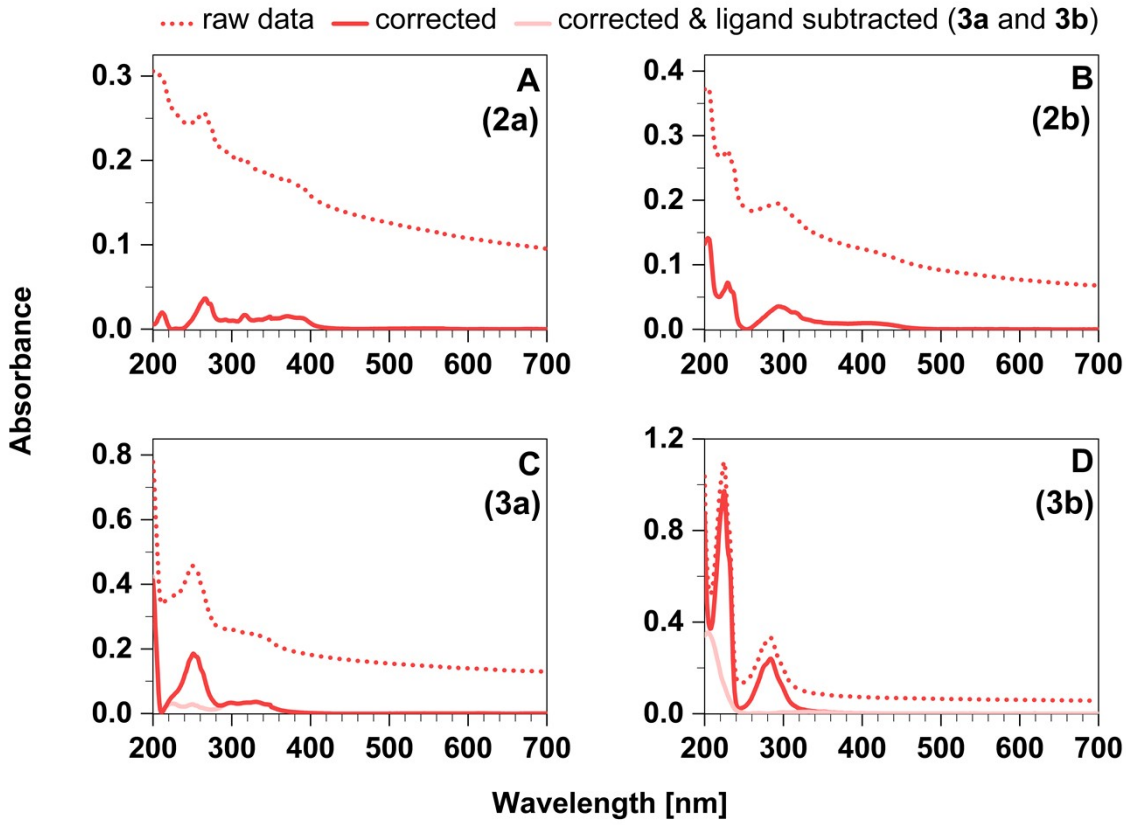

Figure S1. Comparison between raw and corrected absorption spectral data. The applied corrections were described in more detail in the main text under Experimental and Theoretical Procedures.

1.2. Correction of excitation spectra

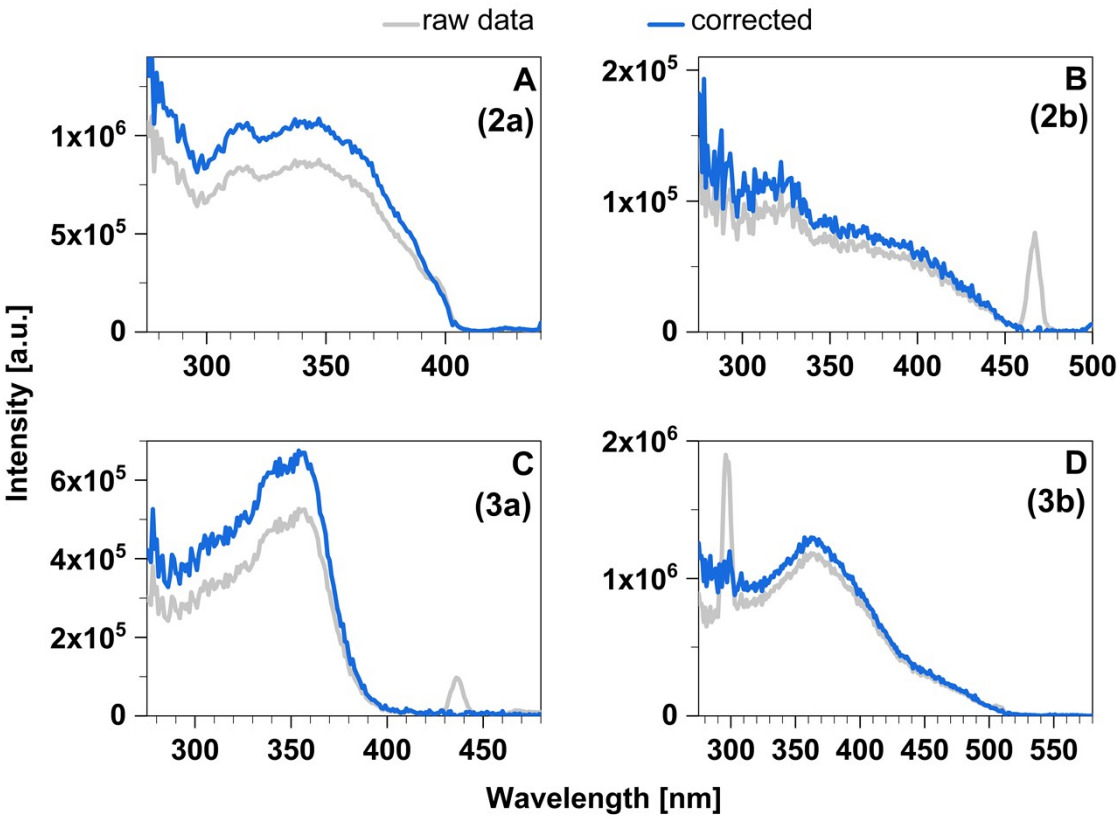

Figure S2. Comparison between raw and corrected excitation spectra. The measured data were corrected for inner filter effect (see Experimental and Theoretical Procedures) and Raman scattering of the solvent. Additionally, the second order diffraction signal of the excitation light was subtracted for **3b**.

1.3. Excitation and emission spectra of powdered samples at 80 K

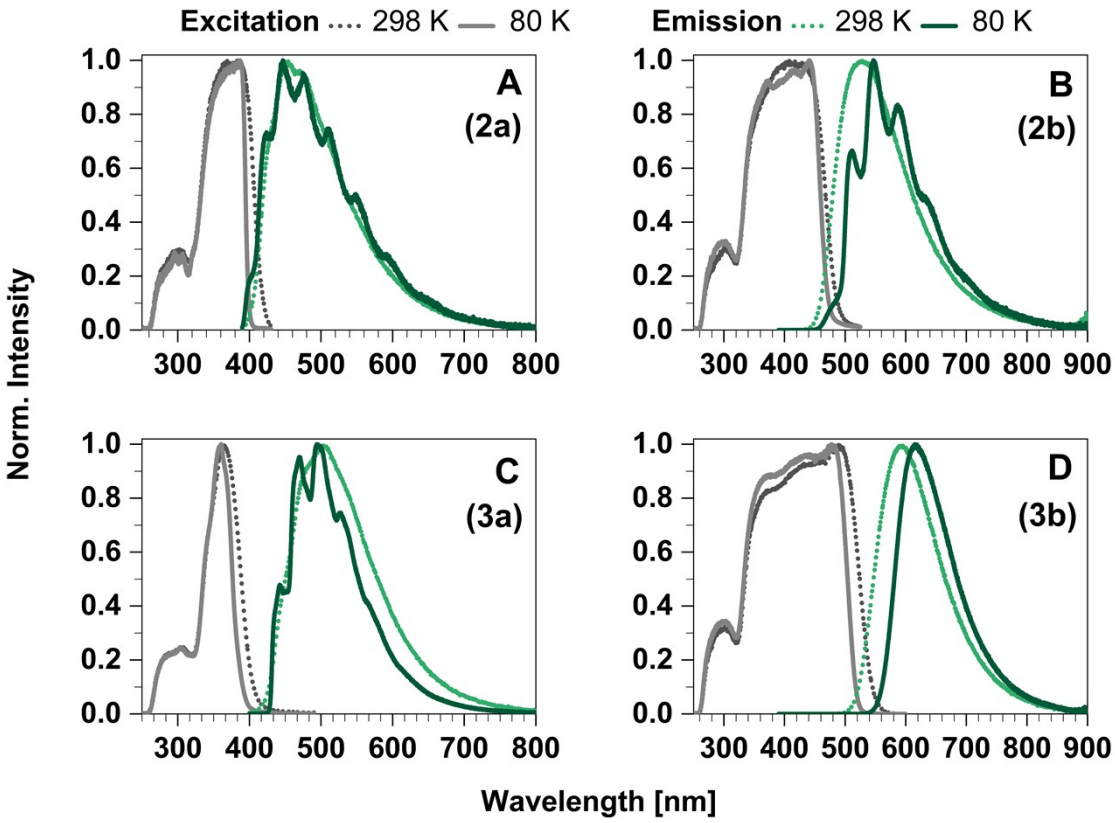

Figure S3. Comparison of the excitation and emission spectra of powdered samples at 298 K and 80 K. The excitation spectra were recorded at emission wavelength of 450 nm (**2a**), 540 nm (**2b**), 500 nm (**3a**), 598 nm (**3b**, 298 K) and 615 nm (**3b**, 80 K). The excitation wavelength was 375 nm for all compounds.

2. Luminescence decays: Temperature series from 10 K to 270 K

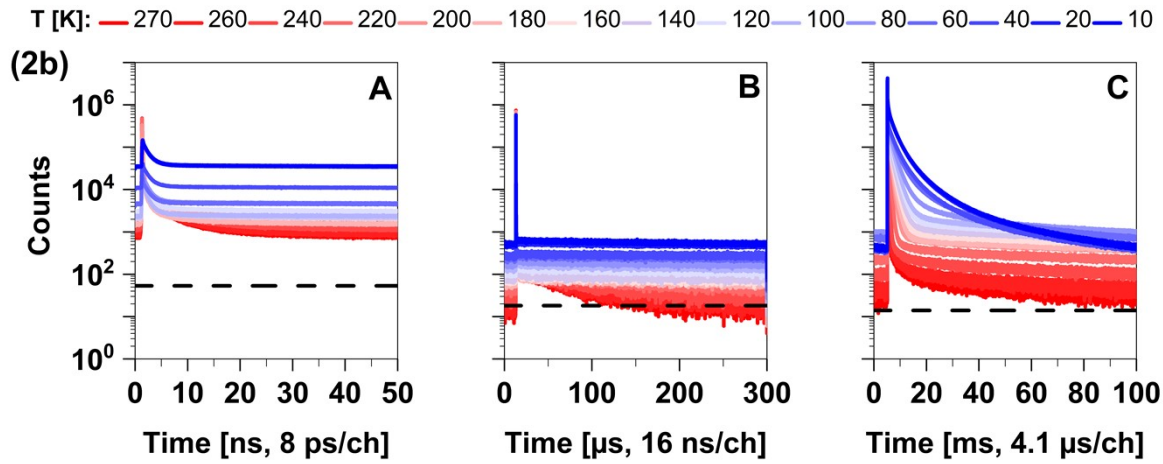

Figure S4. Time-resolved measurements of compound **2b** in solid cyclohexane suspension in the temperature range from 10 K to 270 K, in three distinct time regimes: **A.** nanoseconds, **B.** microseconds, and **C.** milliseconds.

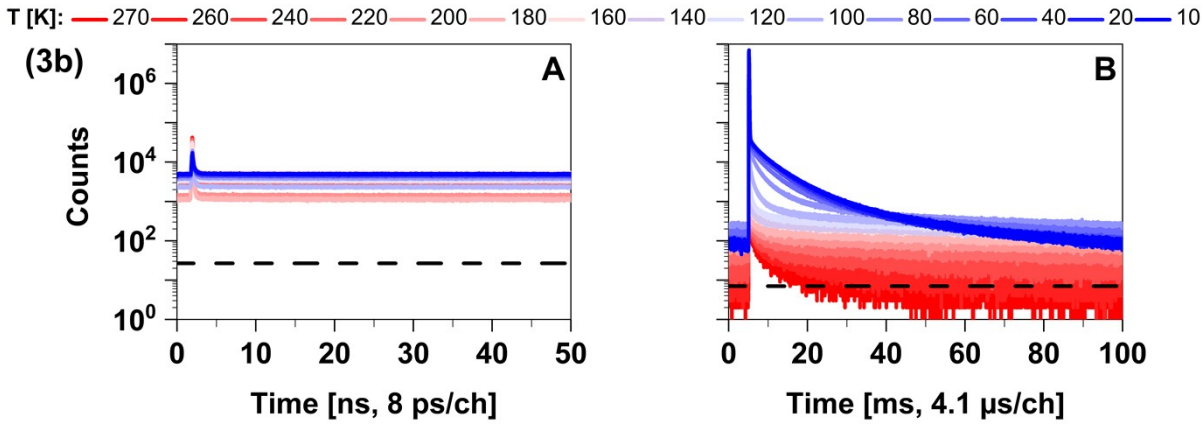

Figure S5. Time-resolved measurements of compound **3b** in solid cyclohexane suspension in the temperature range from 10 K to 270 K, in two distinct time regimes: **A.** nanoseconds, and **B.** milliseconds. The luminescence in milliseconds is assigned to the free ligand (see Chapter 5.2). Decays in microseconds are presented in more detail in Figure S6.

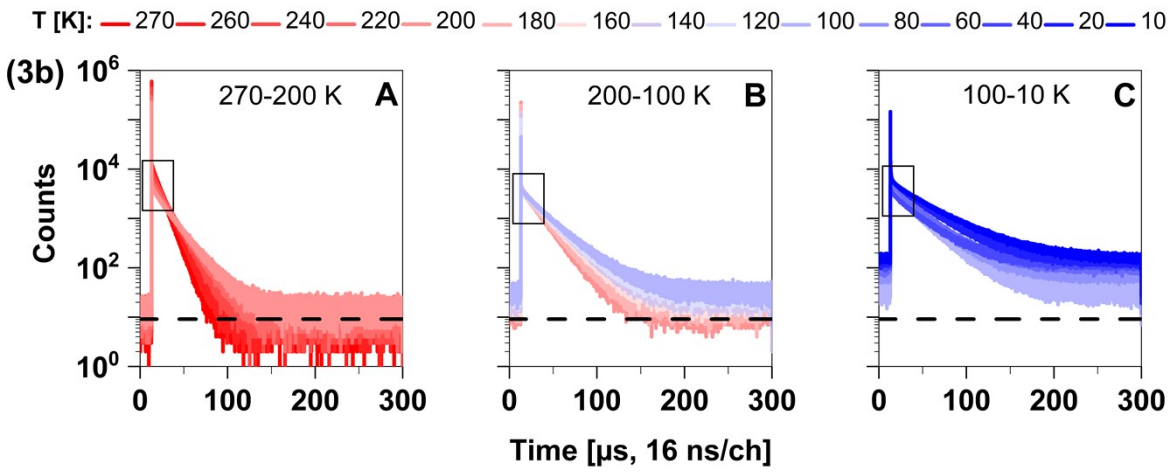

Figure S6. Time-resolved measurements of compound **3b** in solid cyclohexane suspension in microseconds in three characteristic temperature ranges: **A.** 270-200 K, **B.** 200-100 K, and **C.** 100-10 K. In the first temperature range (270-200 K), the amplitude of the delayed emission (marked with a black rectangle) decreases, as is typical for TADF; in the second (200-100 K) it remains constant; while in the third (100-10 K) increases, presumably due to phosphorescence and ligand dissociation.

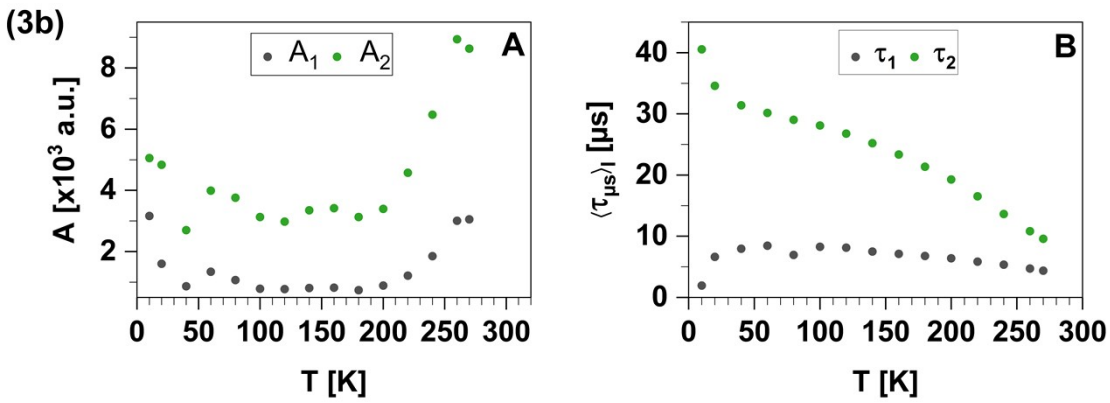

Figure S7. Temperature dependence of **A.** amplitude and **B.** lifetime in the microsecond time range of compound **3b** in solid cyclohexane suspension.

3. Fitting of luminescence decays

A multi-exponential model function (eq. S1) was used to describe the data. For fitting, the model function was convoluted with the instrumental function and, after adding a variable offset, iteratively optimized. For more details, see Experimental and Theoretical Procedures. Each emissive species is presented with its amplitude (A_i) and/or fraction (x_i) (eq. S2), and lifetime (τ_i). Intensity-weighted lifetime $\langle\tau\rangle_I$ (eq. S3) is given, as well as the reduced χ_r^2 value (eq. S4) as a measure of the goodness of the fit. The value $\chi_r^2 = 1$ is obtained with an optimal fit.

$$F(t) = F(0)\sum_{i=1}^{6} x_i e^{-t/\tau_i} \qquad \text{(eq. S1)}$$

$$\sum_{i=1}^{6} x_i = 1 \qquad \text{(eq. S2)}$$

$$\langle\tau\rangle_I = \frac{\sum_{i=1}^{6} x_i \tau_i^2}{\sum_{i=1}^{6} x_i \tau_i} \qquad \text{(eq. S3)}$$

$$\chi_r^2 = \sum_{i=1}^{n} \frac{1}{(n-p)} \times (w.res.)^2 \qquad \text{(eq. S4)}$$

n: number of time channels, p: degrees of freedom

All fit results are given in Table S1 to Table S11.

3.1. The linear lutidine complex **2a**

Table S1. Lifetime fit results of **2a** in cyclohexane suspension in the nanosecond time regime.

T [K]	x_1	**τ_1 [ns]**	x_2	**τ_2 [ns]**	$\langle\tau\rangle_I$ [ns]	χ_r^2
261.3	0.35	**3.30**	0.65	**2.00**	2.61	1.18
163.0	0.48	**5.63**	0.52	**4.28**	5.02	1.14
64.7	0.20	**3.32**	0.80	**6.28**	5.94	1.12
15.1	0.26	**3.55**	0.74	**6.32**	5.87	1.17

Table S2. Lifetime fit results of **2a** in cyclohexane suspension in the millisecond time regime.

T [K]	x_1 $\cdot 10^{-3}$	**τ_1 [ms]**	x_2	**τ_2 [ms]**	x_3	**τ_3 [ms]**	x_4	**τ_4 [ms]**	x_5	**τ_5 [ms]**	$\langle\tau\rangle_I$ [ms]	χ_r^2
261.3	5.9	**13.2**	0.13	**2.27**	0.52	**1.21**	0.34	**0.06**			2.39	1.13
163.0	9.9	**74.4**	0.03	**7.95**	0.17	**1.58**	0.79	**0.08**			43.22	1.06
64.7	8.0	**59.2**	0.07	**11.4**	0.35	**3.73**	0.30	**1.19**	0.28	**0.21**	14.23	1.02

15.1	12.6	**39.1**	0.14	**10.3**	0.49	**4.77**	0.19	**1.37**	0.17	**0.25**	9.96	1.02

3.2. The trigonal pyridine complex **3a**

Table S3. Lifetime fit results of **3a** in cyclohexane suspension in the nanosecond time regime.

T [K]	x_1	**τ_1 [ns]**	x_2	**τ_2 [ns]**	$\langle\tau\rangle_I$ [ns]	χ_r^2
261.4	0.03	**1.18**	0.97	**0.08**	0.45	1.72
163.3	0.04	**1.70**	0.96	**0.11**	0.73	1.15
64.7	0.09	**2.04**	0.91	**0.16**	1.19	1.12
15.2	0.12	**2.47**	0.88	**0.17**	1.70	1.04

Table S4. Lifetime fit results of **3a** in cyclohexane suspension in the microsecond time regime.

T [K]	A_1	x_1	**τ_1 [µs]**	A_2	x_2	**τ_2 [µs]**	$\langle\tau\rangle_I$ [µs]	χ_r^2
261.4	112.2	0.67	**341.20**	55.5	0.33	**6.55**	338.05	1.03
163.3	41.9	0.52	**273.49**	39.3	0.48	**4.12**	269.74	1.01
64.7	79.8	0.33	**219.59**	163.0	0.67	**5.84**	208.57	1.00
15.2	111.5	0.45	**98.68**	138.0	0.55	**6.00**	92.19	1.04

Table S5. Lifetime fit results of **3a** in cyclohexane suspension in the millisecond time regime.

T [K]	x_1 $\cdot 10^{-3}$	**τ_1 [ms]**	x_2	**τ_2 [ms]**	x_3	**τ_3 [ms]**	x_4	**τ_4 [ms]**	x_5	**τ_5 [ms]**	x_6	**τ_6 [ms]**	$\langle\tau\rangle_I$ [ms]	χ_r^2
261.4	0.1	**10.13**	0.48	**0.66**	0.39	**0.44**	0.13	**0.12**					0.58	1.07
163.3	0.3	**165.95**	<0.01	**9.05**	0.55	**1.24**	0.30	**0.62**	0.15	**0.12**			8.59	1.04
64.7	1.5	**73.29**	0.01	**12.69**	0.07	**3.85**	0.49	**1.46**	0.15	**0.45**	0.28	**0.06**	9.01	1.02
15.2	1.8	**42.39**	0.02	**9.82**	0.09	**4.28**	0.26	**1.68**	0.09	**0.29**	0.54	**0.04**	6.76	1.02

3.3. The linear formyl lutidine complex **2b**

Table S6. Lifetime fit results of **2b** in cyclohexane suspension in the nanosecond time regime.

T [K]	x_1 $\cdot 10^{-3}$	τ_1 **[ns]**	x_2 $\cdot 10^{-3}$	τ_2 **[ns]**	x_3	τ_3 **[ns]**	x_4	τ_4 **[ns]**	$\langle\tau\rangle_I$ [ns]	χ_r^2
271.1	0.8	**7.26**	3.3	**1.61**	0.01	**0.39**	0.99	**0.02**	1.57	1.67
261.5	0.8	**7.64**	3.2	**1.61**	0.01	**0.38**	0.99	**0.02**	1.62	1.61
241.7	0.8	**8.53**	3.4	**1.58**	0.01	**0.37**	0.99	**0.02**	1.85	1.65
221.9	0.8	**9.11**	3.5	**1.54**	0.01	**0.38**	0.99	**0.02**	2.01	1.50
202.1	1.0	**10.55**	4.6	**1.61**	0.01	**0.42**	0.98	**0.03**	2.58	1.36
182.6	2.1	**12.13**	9.9	**1.76**	0.03	**0.51**	0.96	**0.04**	3.67	1.04
163.2	7.8	**12.29**	40.6	**1.51**	0.13	**0.54**	0.82	**0.07**	4.59	1.06
143.5	9.0	**18.01**	43.7	**2.12**	0.25	**0.66**	0.69	**0.08**	6.74	1.01
124.0	8.8	**23.42**	32.7	**2.47**	0.34	**0.80**	0.62	**0.05**	8.82	1.03
104.5	6.4	**39.51**	10.8	**4.78**	0.36	**1.01**	0.62	**0.16**	13.85	1.72
84.9	8.6	**24.61**	4.6	**3.87**	0.37	**1.09**	0.62	**0.06**	8.62	1.08
64.7	8.1	**26.64**	0.1	**1.42**	0.30	**1.17**	0.70	**0.07**	10.13	1.08
43.4	11.1	**26.59**	350.1	**1.11**	0.02	**2.21**	0.62	**0.05**	10.97	1.03
25.8	11.0	**43.89**	38.4	**2.37**	0.40	**1.05**	0.56	**0.06**	21.33	1.01
15.1	10.0	**45.60**	32.1	**2.52**	0.37	**1.06**	0.59	**0.05**	22.35	1.02

Table S7. Lifetime fit results of **2b** in cyclohexane suspension in the microsecond time regime.

T [K]	A_1	x_1	τ_1 **[µs]**	A_2	x_2	τ_2 **[µs]**	$\langle\tau\rangle_I$ [µs]	χ_r^2
271.1	111.5	0.56	**50.53**	86.9	0.44	**5.57**	46.97	1.09
261.5	99.5	0.55	**58.45**	81.6	0.45	**4.19**	55.43	1.06
241.7	72.6	0.50	**92.32**	73.1	0.50	**2.82**	89.66	1.05
221.9	57.8	0.40	**124.05**	88.1	0.60	**1.57**	121.73	1.03
202.1	47.4	0.36	**168.66**	84.5	0.64	**1.56**	165.96	1.01
182.6	22.6	0.34	**233.64**	43.2	0.66	**2.31**	229.37	1.02
163.2	18.8	0.35	**272.99**	34.4	0.65	**3.14**	267.41	1.00
143.5	16.9	0.32	**184.00**	35.6	0.68	**2.47**	179.00	1.00
124.0	26.7	0.22	**154.32**	94.3	0.78	**0.48**	152.64	1.00
104.5	30.9	0.13	**194.53**	202.3	0.87	**0.21**	193.15	1.02
84.9	29.4	0.07	**223.40**	381.1	0.93	**0.13**	221.69	1.01
64.7	31.2	0.06	**269.36**	517.1	0.94	**0.13**	267.28	1.02
43.4	32.4	0.05	**393.98**	585.8	0.95	**0.13**	391.60	1.00
25.8	71.8	0.05	**173.95**	1410.4	0.95	**0.13**	171.47	1.02
15.1	110.7	0.06	**202.15**	1855.2	0.94	**0.12**	200.14	1.00

Table S8. Lifetime fit results of **2b** in cyclohexane suspension in the millisecond time regime.

T [K]	$x_1 \cdot 10^{-3}$	**τ_1 [ms]**	$x_2 \cdot 10^{-3}$	**τ_2 [ms]**	$x_3 \cdot 10^{-2}$	**τ_3 [ms]**	x_4	**τ_4 [ms]**	x_5	**τ_5 [ms]**	x_6	**τ_6 [ms]**	$\langle\tau\rangle_{I\,(2\text{-}6)}$ [ms]	χ_r^2
271.1	0.02	**85.6**	0.04	**8.6**	0.02	**1.45**	0.05	**0.11**	0.47	**0.06**	0.47	**0.03**	0.14	1.03
261.5	0.03	**104.8**	0.06	**10.1**	0.03	**1.71**	0.09	**0.15**	0.45	**0.08**	0.46	**0.03**	0.18	1.02
241.7	0.06	**150.4**	0.11	**11.0**	0.05	**1.83**	0.19	**0.27**	0.41	**0.14**	0.40	**0.05**	0.29	1.02
221.9	0.15	**196.4**	0.23	**10.3**	0.65	**1.10**	0.30	**0.47**	0.37	**0.20**	0.32	**0.06**	0.47	1.01
202.1	0.29	**224.8**	0.37	**11.1**	12.13	**1.03**	0.36	**0.62**	0.29	**0.24**	0.22	**0.06**	0.76	1.01
182.6	0.58	**238.4**	0.64	**13.3**	25.93	**1.29**	0.35	**0.77**	0.22	**0.28**	0.18	**0.06**	1.13	1.00
163.2	0.96	**230.2**	0.95	**15.8**	33.49	**1.55**	0.33	**0.96**	0.17	**0.31**	0.16	**0.06**	1.49	0.98
143.5	1.23	**214.2**	1.32	**15.1**	41.29	**1.66**	0.20	**0.93**	0.12	**0.24**	0.26	**0.03**	1.75	1.00
124.0	1.23	**199.9**	1.59	**15.0**	44.61	**1.78**	0.16	**0.95**	0.13	**0.23**	0.26	**0.04**	1.90	1.00
124.0	1.41	**200.6**	1.78	**15.8**	41.64	**1.79**	0.16	**0.99**	0.13	**0.24**	0.29	**0.05**	1.99	1.01
104.5	1.57	**177.3**	3.17	**14.7**	34.61	**2.02**	0.27	**1.31**	0.17	**0.35**	0.21	**0.08**	2.19	1.00
84.9	1.99	**145.6**	8.75	**15.5**	7.01	**3.70**	0.60	**1.78**	0.17	**0.54**	0.15	**0.11**	3.19	1.00
64.7	2.61	**97.2**	19.30	**15.3**	13.29	**4.85**	0.61	**2.02**	0.13	**0.72**	0.10	**0.13**	4.47	1.02
43.4	2.99	**64.7**	27.70	**13.4**	21.90	**4.91**	0.58	**2.07**	0.09	**0.67**	0.08	**0.10**	4.71	0.99
25.8	1.94	**52.3**	21.40	**11.7**	15.90	**4.73**	0.52	**2.00**	0.09	**0.45**	0.21	**0.06**	4.10	0.99
15.1	1.59	**47.7**	23.80	**10.3**	13.23	**4.27**	0.29	**1.88**	0.27	**0.48**	0.28	**0.12**	3.96	0.99

3.4. The trigonal formyl pyridine complex **3b**

Table S9. Lifetime fit results of **3b** in cyclohexane suspension in the nanosecond time regime.

T [K]	$x_1 \cdot 10^{-3}$	**τ_1 [ns]**	x_2	**τ_2 [ns]**	x_3	**τ_3 [$\cdot 10^{-2}$ ns]**	$\langle\tau\rangle_I$ [ns]	χ_r^2
271.5	0.77	**6.10**	0.03	**0.28**	0.97	**5.48**	0.48	1.22
261.6	1.11	**4.69**	0.06	**0.20**	0.94	**4.87**	0.42	1.06
241.8	0.96	**5.44**	0.02	**0.31**	0.97	**6.26**	0.44	1.27
222.0	2.76	**1.53**	0.04	**0.19**	0.95	**5.98**	0.14	1.20
202.2	3.11	**1.90**	0.79	**0.09**	0.21	**0.01**	0.21	1.26
183.1	4.69	**1.28**	0.68	**0.09**	0.31	**0.01**	0.17	1.07
163.3	4.97	**2.17**	0.74	**0.14**	0.25	**0.01**	0.30	1.04
143.6	10.82	**1.27**	0.64	**0.14**	0.35	**0.01**	0.24	1.38
124.1	14.30	**1.09**	0.77	**0.12**	0.22	**0.01**	0.24	1.39
104.6	26.60	**1.10**	0.78	**0.13**	0.19	**0.01**	0.32	1.12
85.0	5.27	**3.16**	0.68	**0.13**	0.31	**0.01**	0.56	1.53
64.8	6.23	**4.78**	0.69	**0.16**	0.30	**0.01**	1.11	1.11
43.5	6.96	**2.57**	0.54	**0.15**	0.45	**0.01**	0.54	1.28
25.8	21.60	**2.43**	0.81	**0.17**	0.17	**0.01**	0.77	1.15
15.0	4.53	**6.19**	0.13	**0.34**	0.87	**5.95**	1.46	1.44

Table S10. Lifetime fit results of **3b** in cyclohexane suspension in the microsecond time regime.

T [K]	A_1	x_1	**τ_1 [µs]**	A_2	x_2	**τ_2 [µs]**	$\langle\tau\rangle_I$ [µs]	χ_r^2
271.3	8634.6	0.74	**9.59**	3051.7	0.26	**4.38**	8.87	1.14
262.0	8941.3	0.75	**10.84**	3006.7	0.25	**4.73**	10.05	1.13
242.3	6474.1	0.78	**13.64**	1846.9	0.22	**5.37**	12.81	1.11
222.4	4575.9	0.79	**16.52**	1212.4	0.21	**5.84**	15.60	1.08
202.7	3391.8	0.79	**19.26**	887.5	0.21	**6.41**	18.23	1.06
185.3	3129.6	0.81	**21.36**	737.1	0.19	**6.78**	20.35	1.05
165.4	3419.2	0.81	**23.36**	819.7	0.19	**7.11**	22.25	1.04
143.8	3345.3	0.81	**25.19**	809.4	0.19	**7.50**	24.00	1.02
124.6	2978.6	0.79	**26.76**	769.9	0.21	**8.12**	25.40	1.03
104.4	3125.3	0.80	**28.09**	783.9	0.20	**8.28**	26.73	1.03
85.1	3758.0	0.78	**29.03**	1064.7	0.22	**6.94**	27.62	1.07
64.8	3990.4	0.75	**30.14**	1338.4	0.25	**8.45**	28.28	1.06
44.1	2701.7	0.76	**31.41**	863.4	0.24	**7.97**	29.65	1.06
25.8	4832.6	0.75	**34.57**	1597.2	0.25	**6.62**	32.90	1.14
15.1	5054.4	0.62	**40.55**	3160.9	0.38	**1.94**	39.42	1.58

Table S11. Lifetime fit results of **3b** in cyclohexane suspension in the millisecond time regime.

T [K]	x_1	**τ_1 [ms]**	x_2	**τ_2 [ms]**	x_3	**τ_3 [ms]**	x_4	**τ_4 [ms]**	$\langle\tau\rangle_I$ [ms]	χ_r^2
271.3			0.13	**10.04**	0.31	**2.30**	0.56	**0.64**	6.31	1.15
262.0	0.06	**38.93**	0.13	**8.13**	0.34	**1.96**	0.47	**0.53**	23.52	1.05
242.3	0.07	**106.53**	0.09	**15.58**	0.29	**3.04**	0.55	**0.77**	80.85	1.05
222.4	0.08	**180.92**	0.09	**14.01**	0.31	**2.56**	0.51	**0.67**	156.86	1.01
202.7	0.07	**295.96**	0.10	**22.27**	0.34	**2.66**	0.49	**0.56**	258.03	1.01
185.3	0.10	**253.31**	0.09	**15.85**	0.35	**2.39**	0.46	**0.49**	231.42	1.02
165.4	0.09	**244.89**	0.09	**16.03**	0.28	**2.51**	0.54	**0.51**	223.24	1.00
143.8	0.07	**228.72**	0.07	**15.66**	0.23	**2.32**	0.63	**0.42**	205.90	0.99
124.6	0.04	**207.14**	0.05	**13.54**	0.17	**2.05**	0.75	**0.44**	177.20	1.01
104.4	0.01	**170.11**	0.03	**11.52**	0.23	**2.00**	0.72	**0.52**	115.25	1.03
85.1	0.01	**123.07**	0.06	**11.69**	0.40	**2.91**	0.52	**0.88**	50.31	1.03
64.8	0.01	**79.65**	0.10	**11.86**	0.57	**3.90**	0.32	**1.35**	21.06	1.01
44.1	0.01	**61.87**	0.09	**12.45**	0.64	**4.66**	0.25	**1.95**	13.24	1.03
25.8	0.01	**51.94**	0.12	**11.03**	0.68	**4.58**	0.19	**1.48**	11.26	1.01
15.1	0.01	**46.68**	0.18	**9.47**	0.51	**4.17**	0.30	**1.01**	10.99	1.03

4. Analysis of luminescence decays

Temperature dependence of prompt fluorescence lifetimes in nanoseconds was approximated according to eq. (1). For more details, see Experimental and Theoretical Procedures. Fit results are given in Table S12.

Table S12. Obtained parameters k_S, k_A and E_A from the fit of temperature-dependent prompt fluorescence lifetimes according to eq. (1).

ns decays	**2a**		**3a**		**2b**		**3b**	
	fit	error [%]	fit	error [%]	fit	error [%]	fit	error [%]
k_S [s^{-1}]	$1.7 \cdot 10^8$	0.6	$5.9 \cdot 10^8$	7.6	$8.5 \cdot 10^8$	2.8	$6.1 \cdot 10^9$	5.2
k_A [s^{-1}]	$5.6 \cdot 10^9$	15.7	$2.5 \cdot 10^9$	36.3	$5.8 \cdot 10^{10}$	57.1	$1.9 \cdot 10^{10}$	48.6
E_A [meV]	73.7	4.3	13.6	26.2	67.3	14.2	26.3	32.2
χ^2	0.0026		0.0152		0.0061		0.0002	
Fraction of total luminescence [%]	99.5		16.9		71.4		6.0	

Temperature dependence of delayed luminescence decay times was approximated according to eq. (2). For **2b**, two models were applied: in the first model, E_2 and E_3 are fixed to theoretically computed zero-point vibrational energy corrected adiabatic values of 28.5 meV and 52.2 meV respectively, while E_1 and E_4 are free parameters (solid line in Figure 9D, Table S13), and in the second model, all four energies E_1-E_4 are fixed (dashed line in Figure 9D, Table S14). Theoretically computed zero-point vibrational energy corrected adiabatic values are provided in Table S15. Zero-field splitting of ^{3}LLCT is <0.09 meV and not relevant in measured temperature range.

Table S13. Obtained fit parameters from temperature-dependent delayed luminescence decay of **2b** in milliseconds according to eq. (2). Fit is depicted as a solid green line in Figure 9D.

2b	Fit	Standard error	Theory	Unit	Assignment
k_0	$2.6 \cdot 10^2$	32		s^{-1}	$^3LLCT_{1,2*} \rightarrow S_0$
k_1	0	fixed		s^{-1}	$^3LLCT_{3*} \rightarrow S_0$
k_2	$4.8 \cdot 10^3$	$3.4 \cdot 10^2$		s^{-1}	$^3LC \rightarrow S_0$
k_3	0	fixed		s^{-1}	$^1LLCT \rightarrow S_0$
k_4	$9.4 \cdot 10^8$	$4.94 \cdot 10^9$		s^{-1}	$^1MLCT \rightarrow S_0$
E_1	3.3	2.9	0.09	meV	^3LLCT zero field splitting
E_2	**28.5**	**fixed**	28.5	meV	$^3LC \rightarrow {}^3LLCT$
E_3	**52.2**	**fixed**	52.2	meV	$^1LLCT \rightarrow {}^3LLCT$
E_4	240.2	102.1	470.3	meV	$^1MLCT \rightarrow {}^3LLCT$
χ^2	0.027				

*Sublevels of ^3LLCT are marked with the corresponding subscripts (1-3).

Table S14. Obtained fit parameters from temperature-dependent delayed luminescence decay of **2b** in milliseconds according to eq. (2). Fit is depicted as a dashed green line in Figure 9D.

2b	Fit	Standard error	Theory	Unit	Assignment
k_0	$3.4 \cdot 10^2$	$6.3 \cdot 10^2$		s^{-1}	$^3LLCT_{1,2} \rightarrow S_0$
k_1	0	$1.3 \cdot 10^3$		s^{-1}	$^3LLCT_3 \rightarrow S_0$
k_2	$4.2 \cdot 10^3$	$1.2 \cdot 10^4$		s^{-1}	$^3LC \rightarrow S_0$
k_3	$1.2 \cdot 10^4$	$2.5 \cdot 10^5$		s^{-1}	$^1LLCT \rightarrow S_0$
k_4	$1.26 \cdot 10^{14}$	$1.48 \cdot 10^{14}$		s^{-1}	$^1MLCT \rightarrow S_0$
E_1	**0.09**	**fixed**	0.09	meV	^3LLCT zero field splitting
E_2	**28.5**	**fixed**	28.5	meV	$^3LC \rightarrow {}^3LLCT$
E_3	**52.2**	**fixed**	52.2	meV	$^1LLCT \rightarrow {}^3LLCT$
E_4	**470.3**	**fixed**	470.3	meV	$^1MLCT \rightarrow {}^3LLCT$
χ^2	0.075				

Table S15. Zero-point vibrational energy corrected adiabatic energies of **2b**.

State	E (0-0) [eV]	ZFS [cm^{-1}]
S_0	0.00	
^{1}LLCT	2.47	
^{3}LLCT	2.42	0.35
^{1}MLCT	2.89	
^{3}LC	2.45	0.26

Temperature dependence of delayed luminescence decay times in microseconds of **3b** was also approximated according to eq. (2). For more details, see Experimental and Theoretical Procedures. Fit results are presented in Table S16. Zero field splitting of ^{3}MLCT has no effect on Boltzmann factor.

Table S16. Obtained fit parameters from temperature-dependent delayed luminescence decay of **3b** in microseconds according to eq. (2). Fit is depicted as a green line in Figure 16D.

	Fit		**Theory**		
3b	$\boldsymbol{k_r + k_{nr}}$**[a]**	**Standard error**	$\boldsymbol{k_r}$ **(77 K)**	**Unit**	**Assignment**
k_0	0	$2.46 \cdot 10^3$	$1.4 \cdot 10^4$	s^{-1}	$^3LLCT_{1,2} \rightarrow S_0$
k_1	$1.09 \cdot 10^5$	$6.72 \cdot 10^3$		s^{-1}	$^3LLCT_3 \rightarrow S_0$
k_2	$6.39 \cdot 10^4$	$4.36 \cdot 10^3$	$7.9 \cdot 10^3$	s^{-1}	$^3MLCT \rightarrow S_0$
k_3	0	$2.14 \cdot 10^4$	$4.2 \cdot 10^5$	s^{-1}	$^1LLCT \rightarrow S_0$
k_4	$3.65 \cdot 10^7$	$2.32 \cdot 10^6$	$2.6 \cdot 10^6$	s^{-1}	$^1MLCT \rightarrow S_0$
	Energy differences		**Energy differences**		
E_1	**0.6**	**fixed**	0.6	meV	^{3}LLCT zero field splitting
E_2	**19.2**	**fixed**	19.2	meV	$^3MLCT \rightarrow {}^3LLCT$
E_3	**62.2**	**fixed**	62.2	meV	$^1LLCT \rightarrow {}^3LLCT$
E_4	**114.2**	**fixed**	114.2	meV	$^1MLCT \rightarrow {}^3LLCT$
χ^2	0.311				

[a] k_{nr} adds a displacement by approximately one order a magnitude to theoretical k_r values.

5. Time-resolved luminescence decays in cyclohexane in milliseconds

5.1. Decay-associated spectra at 10 K of the linear formyl lutidine complex **2b**

Decay-associated spectra at 10 K in the millisecond time regime were recorded to determine the spectral properties of each lifetime species. Four lifetimes were used for global fitting: τ_1 = 0.7 ms, τ_2 = 1.9 ms, τ_3 = 5.6 ms, and τ_4 = 20.0 ms. The amplitudes A_3 and A_4 resemble the spectral properties of the free ligand (Figure S8A) shown in Figure 8B. At a detection wavelength of 460 nm, the lifetime of 5.6 ms assigned to the free ligand contributes to a substantial fraction of the total emission, accounting for 63% of the emission intensity. In contrast, the very long lifetime of 20.0 ms represents only 6% of the total emission at the same wavelength. The situation changes when the detection wavelength is shifted to the detection maximum of the compound, 540 nm. At this wavelength, the lifetime of 5.6 ms contributes only 2% of the total emission, while the lifetime of 20.0 ms contributes a mere 0.1% of the total emission. This indicates that the majority of the emission in the millisecond time regime, detected at 540 nm, originates from complex **2b** and not from the free ligand (Figure S8B).

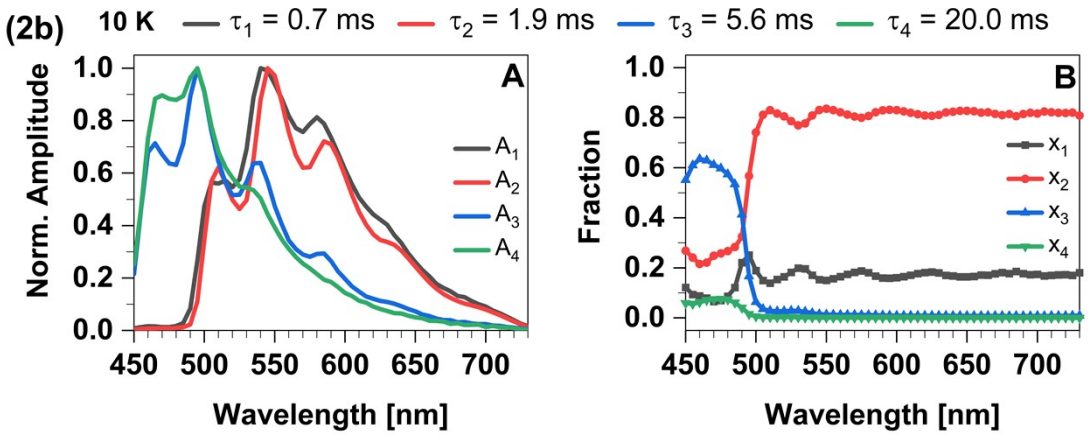

Figure S8. Decay-associated spectra of **2b** in cyclohexane suspension at 10 K in the millisecond time range. The lifetimes used for global fitting were τ_1 = 0.7 ms, τ_2 = 1.9 ms, τ_3 = 5.6 ms, and τ_4 = 20.0 ms. **A.** Spectral properties of each lifetime species with their normalized amplitudes. **B.** Fraction dependence on the wavelength.

5.2. Decay-associated spectra at 10 K of the trigonal formyl pyridine complex **3b**

A small portion of the total luminescence signal is detected in the millisecond time regime at all temperatures, in particular below 100 K. By integrating the histogram spike at 10 K, which contains shorter lifetime components, we identified the spectrum of the compound. However, the integration of the histogram tail at the same temperature, revealed the spectrum of the free ligand (Figure S9A). Additionally, we constructed the decay-associated spectra at 10 K using individual lifetimes, and it is evident that all these spectra originate from the dissociated ligand (Figure S9B). The structured band, appearing also at the short wavelength tail of the steady-state emission spectrum at temperatures below 100 K (Figure 14), is assigned to luminescence from the nπ* state of the free 4-formyl pyridine ligand. The millisecond emission was not observed in solid-state measurements as there is no ligand dissociation in the powder sample.

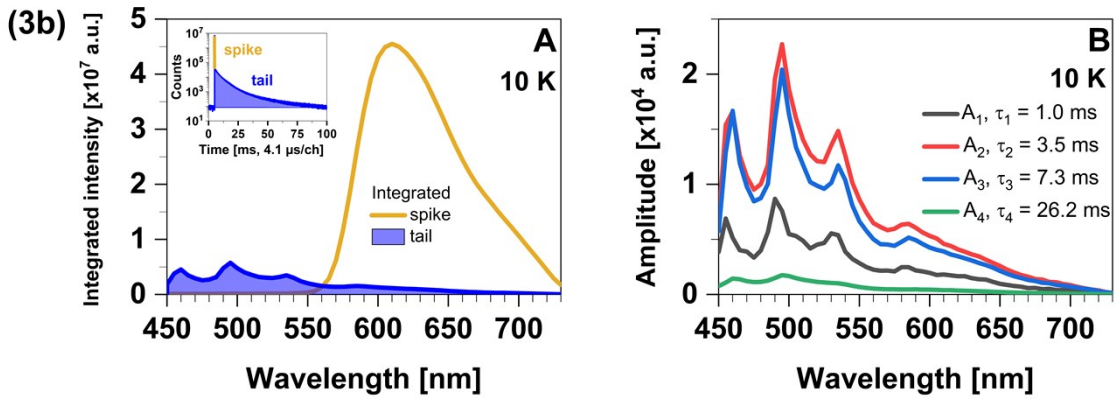

Figure S9. Time-resolved measurements of **3b** in cyclohexane suspension in the millisecond time regime. **A.** Time-resolved emission spectra constructed by the integration of the spike and tail of the decay histogram in the millisecond time range at 10 K. Inset: Decay recorded at 10 K with marked integrated areas. **B.** Decay-associated spectra at 10 K reveal that all four lifetime components have the same spectral properties that match the free ligand emission.

6. Time-resolved luminescence of the free ligand in cyclohexane solution

6.1. Free ligand of compound **2b**: 4-formyl-2,6-lutidine

The complicated multi-exponential behaviour of **2b** observed in the millisecond time range can be attributed to the emission of two distinct species: compound **2b** and its free ligand (4-formyl-2,6-lutidine). The ligand does not interfere with the emission of the compound in nanoseconds and microseconds, as it remains non-emissive in these time regimes (Figure S10, A and B). However, it contributes to the emission observed in the millisecond time range (Figure S10C). The lifetime constants and their fractions are presented in Table S17.

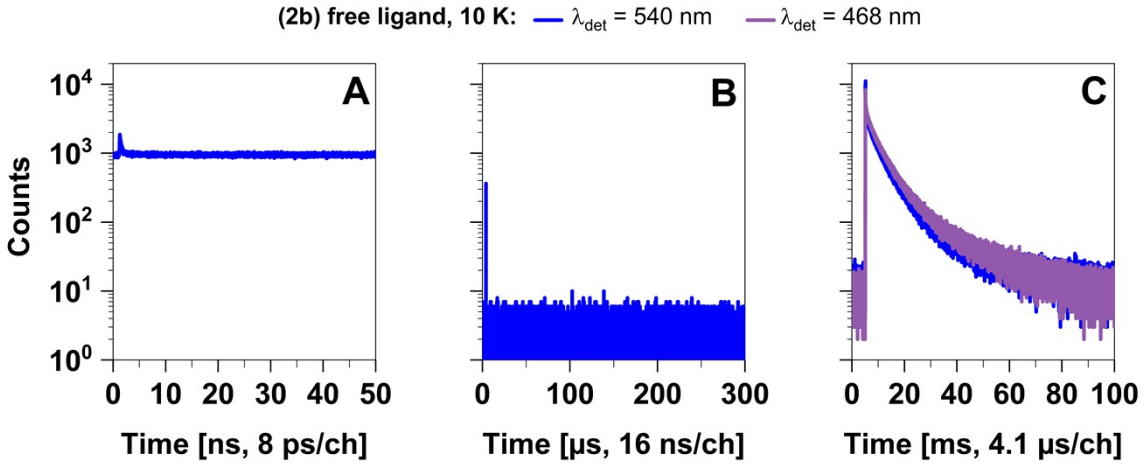

Figure S10. Time-resolved measurements of **2b** free ligand (4-formyl-2,6-lutidine) in cyclohexane solution at 10 K in three-time regimes: **A.** nanoseconds; **B.** microseconds; and **C.** milliseconds.

Table S17. Free ligand (4-formyl-2,6-lutidine) in cyclohexane solution in milliseconds at 10 K. The decays were recorded at two detection wavelengths: 540 nm (emission maximum of the compound) and 468 nm (emission maximum of the free ligand).

λ_{det}	x_1	τ_1 [ms]	x_2	τ_2 [ms]	x_3	τ_3 [ms]	x_4	τ_4 [ms]	$\langle\tau\rangle_I$ [ms]	χ_r^2
468	0.02	**31.96**	0.30	**7.39**	0.36	**3.09**	0.31	**0.39**	9.82	1.05
540	0.02	**26.18**	0.37	**6.28**	0.29	**2.34**	0.32	**0.31**	8.50	1.04

6.2. Free ligand of compound **3b**: 4-formyl pyridine

The free ligand of **3b** complex, 4-formyl pyridine, has an emission maximum at 465 nm. The emission band features strong vibronic coupling at very low temperatures (10-80 K). Time-resolved measurements are conducted at 10 K at the detection maximum of the free ligand (465 nm). As for **2b**, the ligand does not obscure the emission of the compound in the nanosecond and microsecond time regimes, but it affects the millisecond time regime (Figure S11). In the millisecond time regime, the decays were recorded at 465 nm and at the detection maximum of the compound, 595 nm. Similar lifetime constants were obtained at both detection wavelengths (Table S18), indicating the emission of a single species in this time regime.

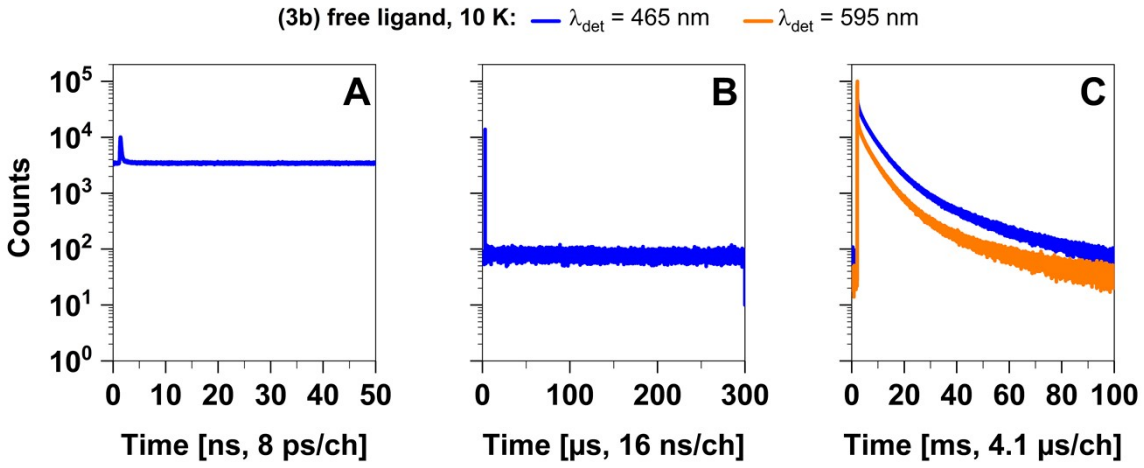

Figure S11. Time-resolved measurements of free ligand (4-formyl pyridine) in cyclohexane solution at 10 K in three-time regimes: **A.** nanoseconds; **B.** microseconds; and **C.** milliseconds.

Table S18. Free ligand (4-formyl pyridine) in cyclohexane solution in the millisecond time regime at 10 K. The decays were recorded at two detection wavelengths: 465 nm (emission maximum of the free ligand) and 595 nm (emission maximum of the compound).

λ_{det}	x_1	τ_1 [ms]	x_2	τ_2 [ms]	x_3	τ_3 [ms]	x_4	τ_4 [ms]	$\langle\tau\rangle_I$ [ms]	χ_r^2
465	0.02	**36.65**	0.26	**8.49**	0.46	**3.64**	0.26	**0.56**	10.96	1.13
595	0.01	**42.69**	0.26	**7.80**	0.43	**3.29**	0.30	**0.47**	10.39	1.07

7. Time-resolved measurements of powdered samples

Table S19. Summary of the lifetime fit results of powdered **2a**, **2b**, **3a** and **3b.**

Compound	T [K]	x_1	τ_1	x_2	τ_2	x_3	τ_3	$\langle\tau\rangle_x$	$\langle\tau\rangle_I$	unit	χ_r^2
2a	298	0.40	**2.09**	0.60	**1.22**	-	-	1.57	1.69	**ns**	1.17
		0.89	**1.27**	0.11	**0.56**	-	-	1.19	1.23	**ms**	1.19
	80	0.99	**5.76**	<0.01	**1.73**	-	-	5.79	5.85	**ns**	3.21
		0.88	**2.28**	0.12	**1.22**	-	-	2.15	2.21	**ms**	1.14
2b	298	0.01	**11.84**	0.40	**2.88**	0.59	**1.21**	2.11	3.51	**ns**	1.27
		<0.01	**24.03**	<0.01	**6.22**	0.99	**0.35**	0.39	1.67	**µs**	1.05
	80	0.04	**42.33**	0.15	**4.68**	0.81	**1.21**	3.36	22.28	**ns**	1.03
		<0.01	**1.45**	<0.01	**0.47**	0.99	**0.02**	0.02	0.04	**ms**	1.12
3a	298	<0.01	**7.28**	0.56	**0.44**	0.44	**0.24**	0.36	0.40	**ms**	1.22
	80	0.32	**1.70**	0.39	**0.98**	0.29	**0.20**	0.98	1.32	**ms**	1.13
3b	298	1.00	**7.58**	-	-	-	-	7.58	7.58	**µs**	1.07
	80	<0.01	**130.37**	0.77	**28.76**	0.23	**12.96**	25.18	27.42	**µs**	1.11

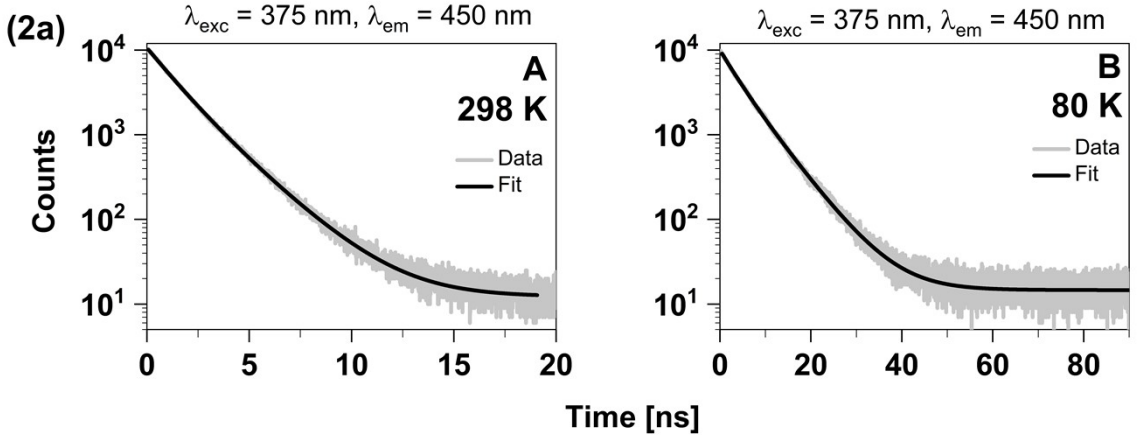

Figure S12. Time-resolved decays of **2a** (powdered sample) in the nanosecond range at two different temperatures: **A.** 298 K and **B.** 80 K.

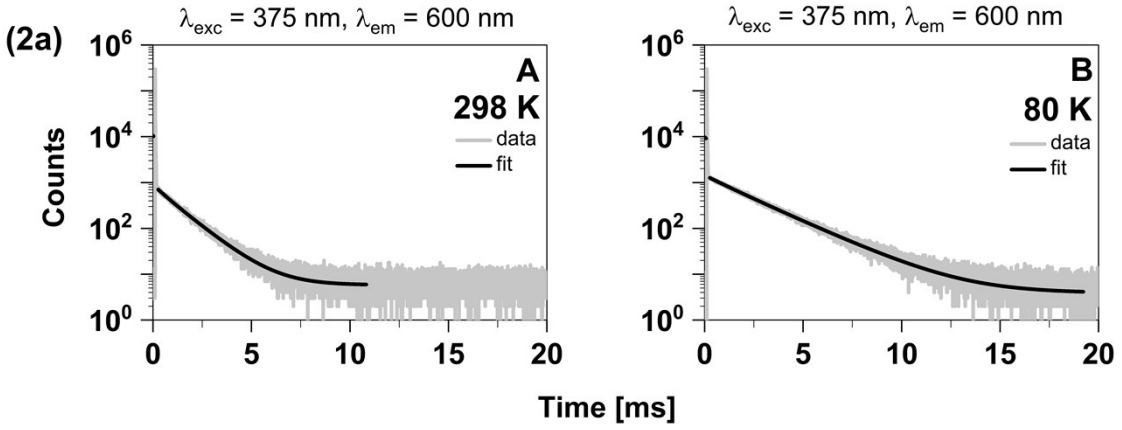

Figure S13. Time-resolved decays of **2a** (powdered sample) in the millisecond range at two different temperatures: **A.** 298 K and **B.** 80 K.

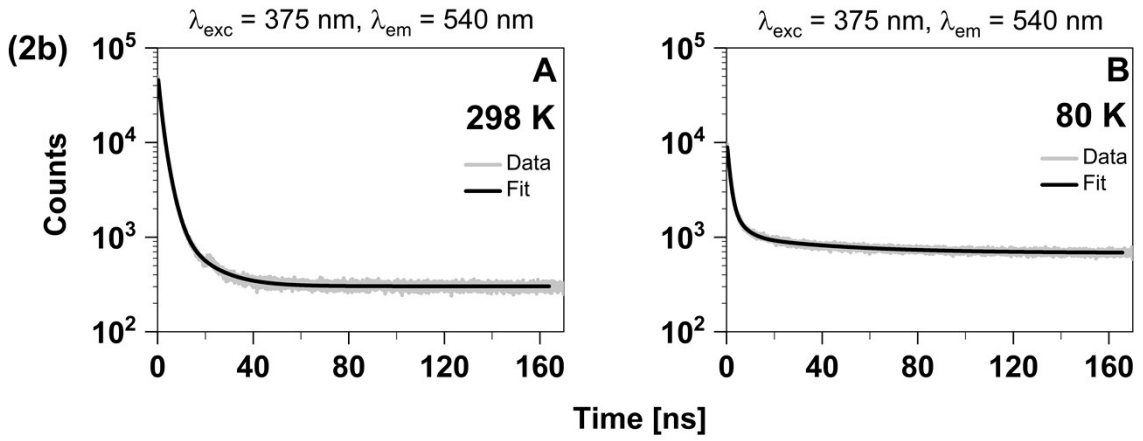

Figure S14. Time-resolved decays of **2b** (powdered sample) in the nanosecond range at two different temperatures: **A.** 298 K and **B.** 80 K.

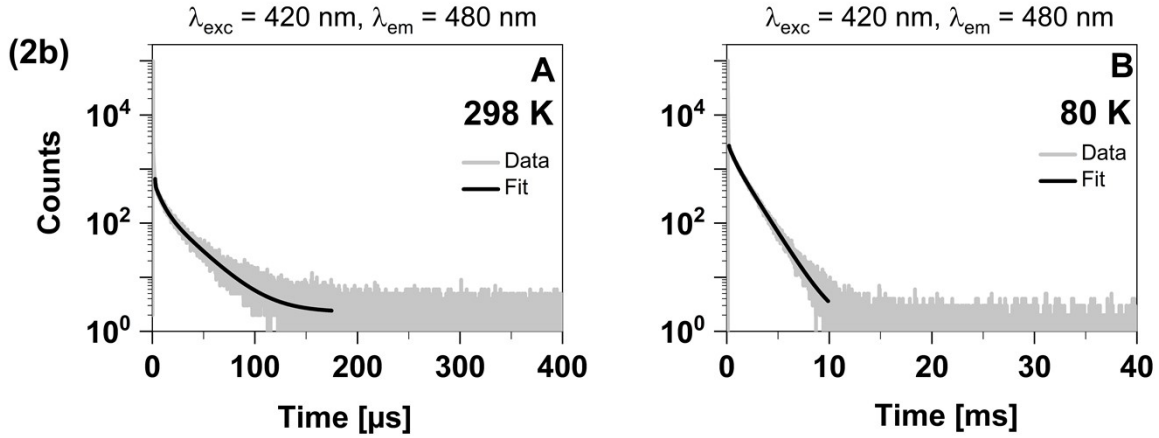

Figure S15. Time-resolved decays of **2b** (powdered sample) in two different time ranges and at two different temperatures: **A.** microseconds, 298 K and **B.** milliseconds, 80 K.

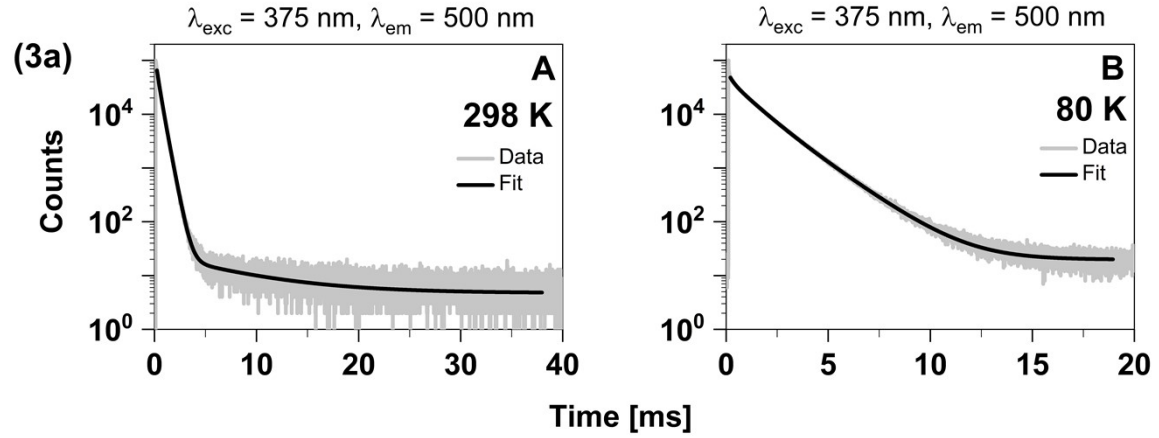

Figure S16. Time-resolved decays of **3a** (powdered sample) in the millisecond range at two different temperatures: **A.** 298 K and **B.** 80 K.

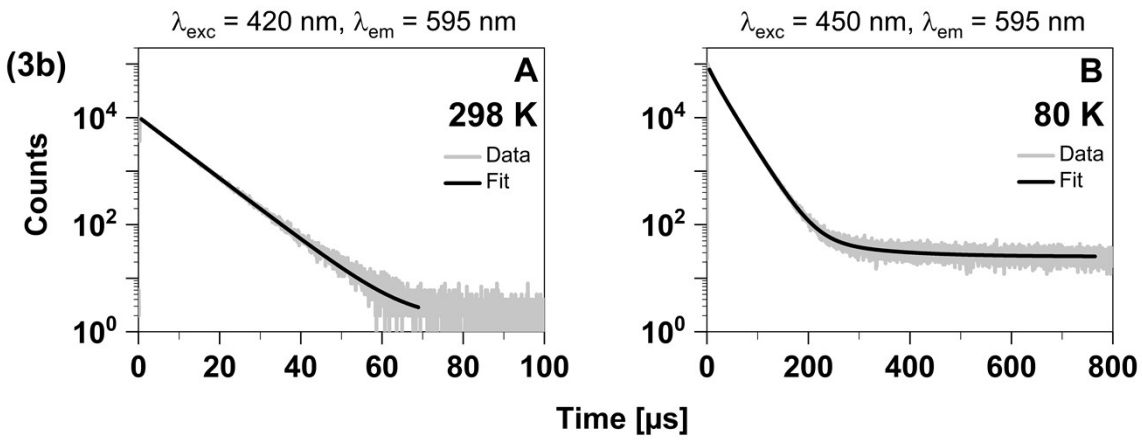

Figure S17. Time-resolved decays of **3b** (powdered sample) in the microsecond range at two different temperatures: **A.** 298 K and **B.** 80 K.

8. Detailed computational results

8.1. Computed photophysical data

Table S20. Extended calculated photophysical data of the complexes **2a**, **3b**, **3a**, **3b**.

Property	Compound			
	2a	**2b**	**3a**	**3b**
$\Delta E_{0\text{-}0}$ [eV]	0.582 (LC)	0.052 (LLCT) -0.023 (^{1}LLCT-^{3}LC)	0.463 (LC)	0.062 (LLCT) 0.095 (MLCT)
$\lambda_{aem,adia}$ [nm]	409 (^{1}LC) [b] 519 (^{3}LC)	497 (^{1}LLCT) 507 (^{3}LLCT) 497 (^{3}LC)	372(^{1}LLCT) 389(^{1}MLCT) 391(^{1}LC) 405 (^{3}MLCT) 459 (^{3}LC)	516 (^{1}LLCT) 529 (^{3}LLCT) 519 (^{1}MLCT) 541 (^{3}MLCT)
$\lambda_{em,vert}$ [a] [nm]	443 (^{1}LC)[b] 664 (^{3}LC)	563 (^{1}LLCT) 591 (^{3}LLCT) 615 (^{3}LC)	422 (^{1}LLCT) 485 (^{1}MLCT) 606 (^{1}LC) 525 (^{3}MLCT) 665 (^{3}LC)	704 (^{1}LLCT) 728 (^{3}LLCT) 707 (^{1}MLCT) 748 (^{3}MLCT)
λ_{abs} (S_1) [nm]	349 (LC/LLCT)	412 (LLCT)	329 (LLCT/MLCT(d_{xz}))	452 (LLCT/MLCT(d_{xz}))
λ_{abs} (T_1) [nm]	390 (LC)	426 (LLCT+LC)	347 (LC)	465 (LLCT+MLCT)
f_{abs} (S_1)	0.09251	0.03057	0.00916	0.01507
k_F (298 K) [s^{-1}]	4.0×10^7 (^{1}LC)[b]	6.3×10^6 (^{1}LLCT)	5.9×10^6 (^{1}LLCT) 1.0×10^7 (^{1}MLCT) 1.0×10^7 (SLC)	4.2×10^5 (^{1}LLCT) 2.6×10^6 (^{1}MLCT)
k_P (77 K) [s^{-1}]	1.1×10^1 (^{3}LC)	7.6×10^1 (^{3}LLCT) 2.7×10^1 (^{3}LC)	9.5×10^3 (^{3}MLCT) 8.6×10^1 (TLC)	1.4×10^4 (^{3}LLCT) 7.9×10^3 (^{3}MLCT)
kISC (298 K) [s^{-1}]	8.0×10^7 (^{1}LC - ^{3}LC)[b]	2.7×10^6 (^{1}LLCT - ^{3}LLCT) 8.5×10^5 (^{1}LLCT - ^{3}LC)	1.5×10^9 (^{1}LC - ^{3}LC) 5.8×10^9(^{1}MLCT - ^{3}MLCT) 7.2×10^9 (^{1}LLCT - ^{3}MLCT)	2.3×10^7 (^{1}LLCT - ^{3}LLCT) 9.1×10^{10} (^{1}LLCT - ^{3}MLCT) 2.7×10^{10} (^{1}MLCT - ^{3}MLCT) 2.8×10^{11} (^{1}MLCT - ^{3}LLCT)
krISC (298 K) [s^{-1}]	-	1.0×10^5 (^{3}LLCT - ^{1}LLCT) 1.8×10^3 (^{3}LC - ^{1}LLCT)	5.1×10^{-2} (^{3}LC - ^{1}LC) 4.4×10^8 (^{3}MLCT - ^{1}MLCT) -	3.1×10^5 (^{3}LLCT - ^{1}LLCT) 2.1×10^9 (^{3}MLCT - ^{3}LLCT) 5.7×10^8 (^{3}MLCT - ^{1}MLCT) 2.4×10^8 (^{3}LLCT - ^{1}MLCT)
kISC (77 K) [s^{-1}]	1.7×10^7 (^{1}LC - ^{3}LC)[b]	3.4×10^6 (^{1}LLCT - ^{3}LLCT) 6.2×10^5 (^{1}LLCT - ^{3}LC)	1.4×10^9 (^{1}LC - ^{3}LC) 4.7×10^9 (^{1}MLCT - ^{3}MLCT) 1.2×10^{10} (^{1}LLCT - ^{3}MLCT)	5.8×10^6 (^{1}LLCT - ^{3}LLCT) 1.8×10^{11} (^{1}LLCT - ^{3}MLCT) 1.5×10^{10}(^{3}MLCT - ^{3}MLCT 1.4×10^{12} (^{3}MLCT - ^{3}LLCT)
krISC (77 K) [s^{-1}]	-	4.9×10^2 (^{3}LLCT - ^{1}LLCT) 5.1×10^2 (^{3}LC - ^{1}LLCT)	- - -	8.9×10^1 (^{3}LLCT - ^{1}LLCT) 1.8×10^7 (^{3}MLCT - ^{1}LLCT) 8.8×10^3 (^{3}MLCT - ^{1}MLCT) 9.4×10^3 (^{3}LLCT - ^{1}MLCT)

[a]Multiple entries indicate that more than one minimum was found on the S_1 or T_1 potential energy hypersurface, respectively. Adiabatic excitation energies and photophysical properties at these minima are given in the ESI.

[b]The ^{1}LC state was optimized with the constrained inter-ligand dihedral angle of the ^{3}LC state. It does not constitute a proper minimum on the S_1 potential energy hypersurface. A proper minimum could not be obtained with the PBE0 functional.

8.2. Vibes parameters

Table S21. Parameters utilized in the computation of the intersystem crossing rates with the VIBES program. If the rate is not mentioned in the table below, an interval of 3000 fs and a damping (eta) of 10 cm^{-1} were used.

Compound	from	to	T [K]	Interval [fs]	Eta [cm^{-1}]
2b	SLLCT	TLC	298	1000	10
	SLLCT	TLC	77	1000	10
	TLC	SLLCT	298	1000	10
3a	TLC	SLC	298	3000	1
	SLLCT	TMLCT	298	500	10
	SLLCT	TMLCT	77	500	10
	TLLCT	SLLCT	77	1000	10
3b	SLLCT	TMLCT	298	300	10
	SLLCT	TMLCT	77	1000	20
	TMLCT	SLLCT	298	100	10
	TMLCT	SLLCT	77	300	10
	TLLCT	SMLCT	298	1000	10
	TLLCT	SMLCT	77	1000	10

8.3. The linear lutidine complex **2a**

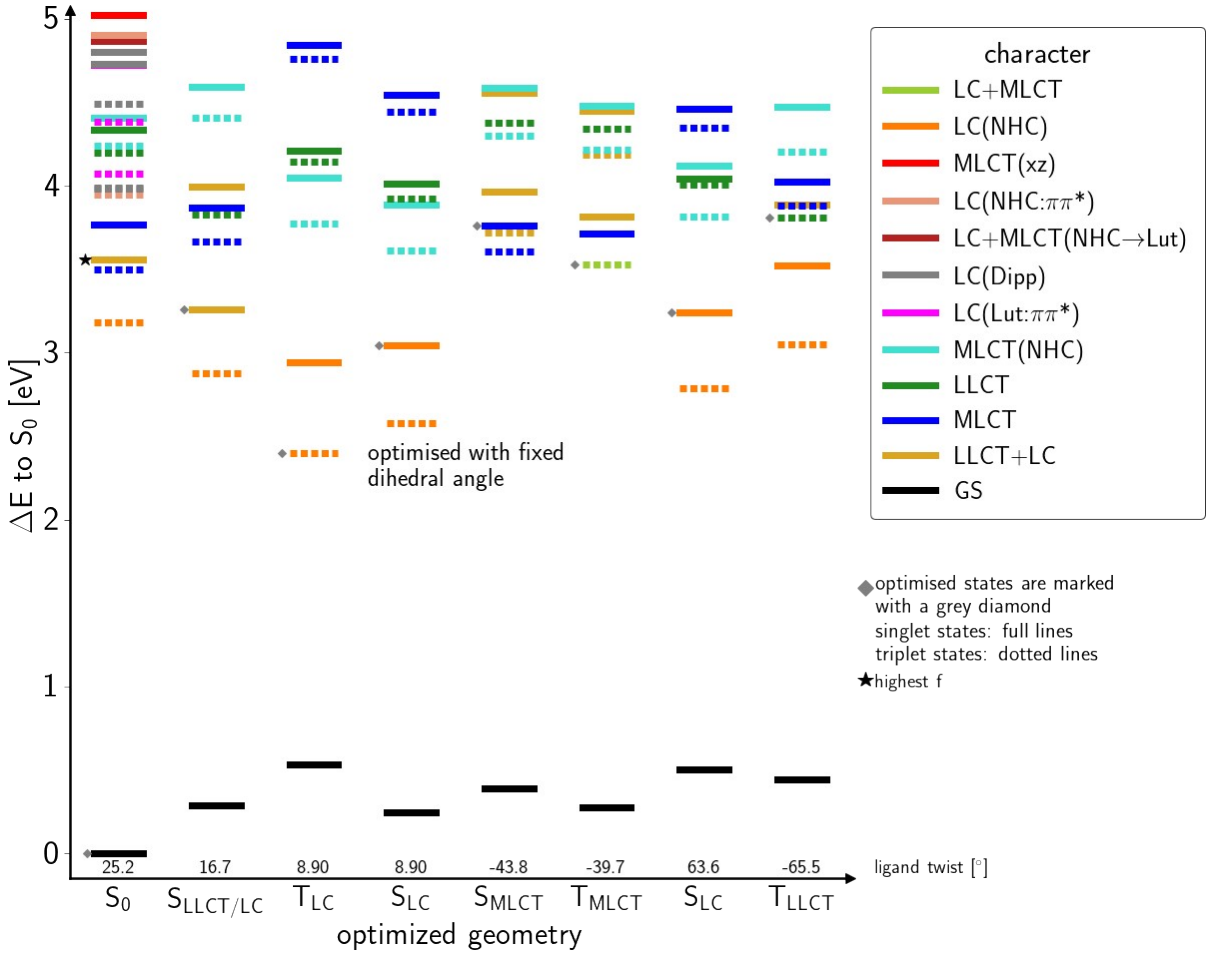

Figure S18. Energy state diagram of **2a** for selected optimized geometries.

Table S22. Singlet states and their properties at the ground state geometry of **2a**.

State	E [eV]	λ_{abs} [nm]	f	|μ| [D]	Character
S0	0			19.21	S0
S1	3.557	349	0.09251	4.79	LLCT+LC
S2	3.767	329	0.02394	14.76	MLCT
S3	4.333	286	0.00585	6.41	LLCT
S4	4.408	281	0.00218	15.07	MLCT(NHC)
S5	4.726	262	0.09399	18.05	LC(Lut:ππ*)
S6	4.728	262	0.00529	17.22	LC(Dipp)
S7	4.804	258	0.00483	19.16	LC(Dipp)
S8	4.866	255	0.01983	12.71	LC+MLCT(NHC →Lut)
S9	4.902	253	0.05730	12.21	LC(NHC:ππ*)
S10	5.021	247	0.10468	13.32	MLCT(xz)

Table S23. Triplet states and their properties at the ground state geometry of **2a**.

State	E [eV]	-	-	|μ| [D]	Character
T1	3.180			8.06	LC(NHC)
T2	3.5499			17.80	MLCT
T3	3.947			16.48	LC(NHC:ππ*)
T4	3.981			19.23	LC(Dipp)
T5	3.987			19.17	LC(Dipp)
T6	4.073			19.44	LC(Lut:ππ*)
T7	4.296			4.81	LLCT
T8	4.239			12.00	MLCT(NHC)
T9	4.382			13.79	LC(Lut:ππ*)
T10	4.490			18.95	LC(Dipp)

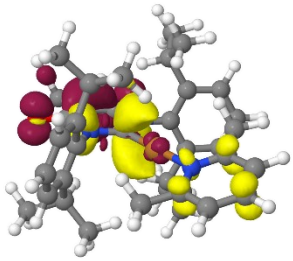

Figure S19. S1-S0 difference density at the **2a** GS.

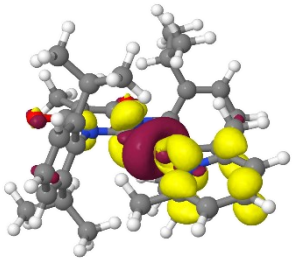

Figure S20. S2-S0 difference density at the **2a** GS.

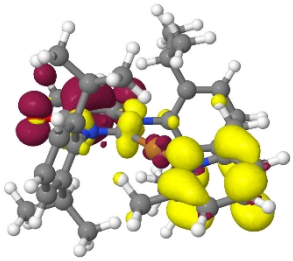

Figure S21. S3-S0 difference density at the **2a** GS.

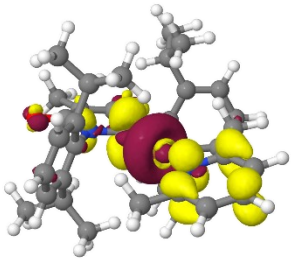

Figure S22. S4-S0 difference density at the **2a** GS.

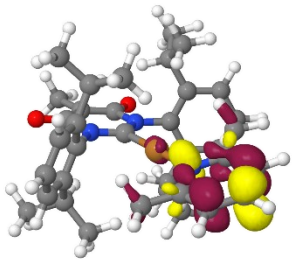

Figure S23. S5-S0 difference density at the **2a** GS.

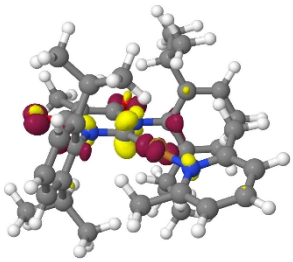

Figure S24. S6-S0 difference density at the **2a** GS.

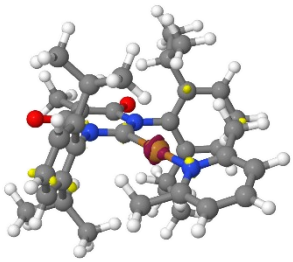

Figure S25. S7-S0 difference density at the **2a** GS.

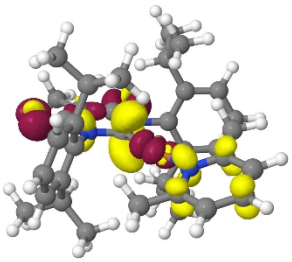

Figure S26. S8-S0 difference density at the **2a** GS.

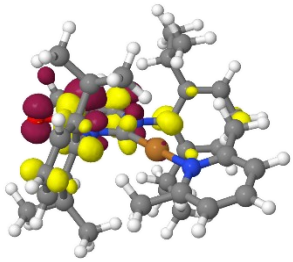

Figure S27. S9-S0 difference density at the **2a** GS.

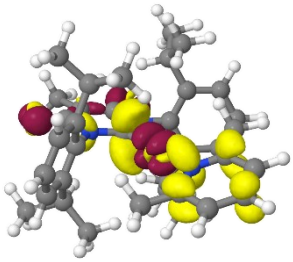

Figure S28. S10-S0 difference density at the **2a** GS.

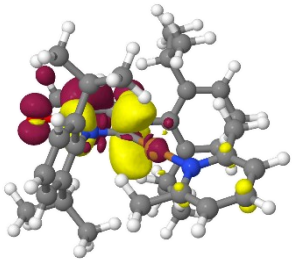

Figure S29. T1-S0 difference density at the **2a** GS.

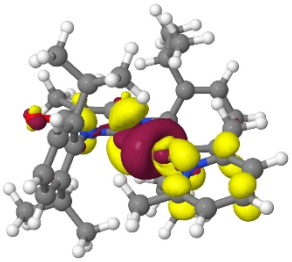

Figure S30. T2-S0 difference density at the **2a** GS.

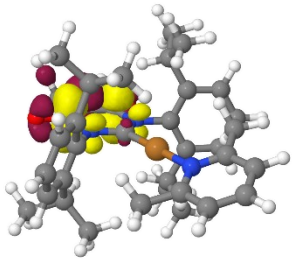

Figure S31. T3-S0 difference density at the **2a** GS.

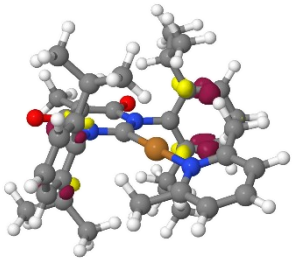

Figure S32. T4-S0 difference density at the **2a** GS.

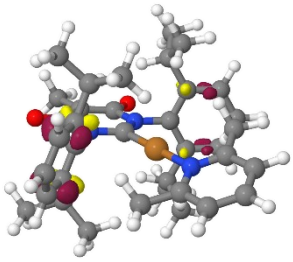

Figure S33. T5-S0 difference density at the **2a** GS.

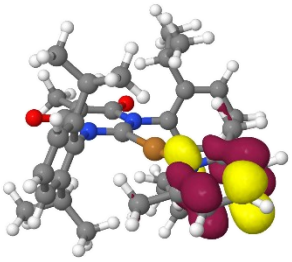

Figure S34. T6-S0 difference density at the **2a** GS.

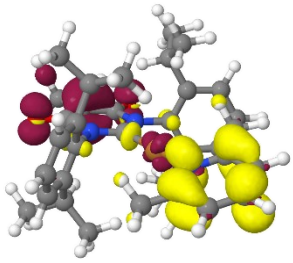

Figure S35. T7-S0 difference density at the **2a** GS.

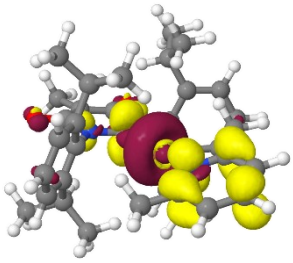

Figure S36. T8-S0 difference density at the **2a** GS.

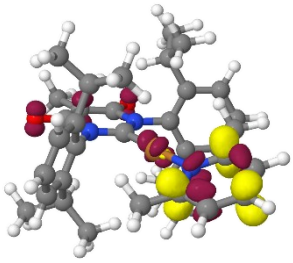

Figure S37. T9-S0 difference density at the **2a** GS.

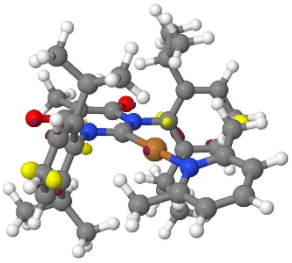

Figure S38. T10-S0 difference density at the **2a** GS.

Table S24. Energies [eV] of relevant excited states of **2a** at the optimized geometries of different states.

State	Optimized geometry							
	S0	SLC-8.9	TLC	SMLCT	TMLCT	TLLCT	SLC/LLCT	SLC-65.6
S0	0.000	0.246	0.531	0.387	0.278	0.445	0.287	0.505
SLC	3.557	3.042	2.943	4.554	3.815	3.521	3.261	3.239
TLC	3.180	2.579	2.397	3.720	4.184	3.050	2.8875	2.7854
SMLCT	3.767	4.550	4.841	3.760	3.711	4.025	3.868	4.459
TMLCT	3.499	4.440	4.760	3.606	3.526	3.879	3.663	4.357
SLLCT	4.333	4.009	4.209	3.963	4.173	3.888	3.994	4.041
TLLCT	4.196	3.923	4.143	4.374	4.185	3.812	3.824	4.001
SMLCT(NHC)	4.408	3.885	4.048	4.588	4.479	4.469	4.594	4.120
TMLCT(NHC)	4.239	3.610	3.771	4.297	4.216	4.205	4.404	3.8112

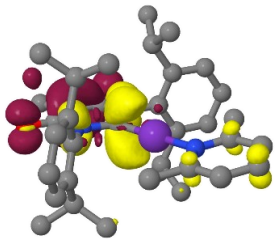

Figure S39. S1-S0 (LC(NHC)) difference density at the **2a** SLC-8.9geometry.

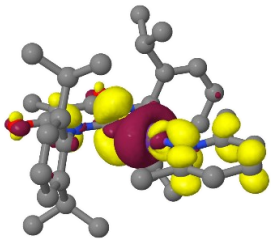

Figure S40. S2-S0 (MLCT(NHC)) difference density at the **2a** SLC-8.9 geometry.

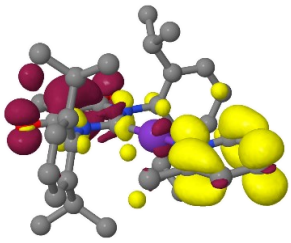

Figure S41. S3-S0 (LLCT) difference density at the **2a** SLC-8.9 geometry.

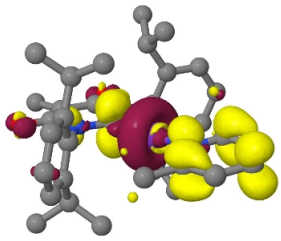

Figure S42. S5-S0 (MLCT) difference density at the **2a** SLC-8.9 geometry.

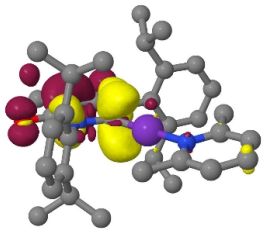

Figure S43. T1-S0 (LC(NHC)) difference density at the **2a** SLC-8.9 geometry.

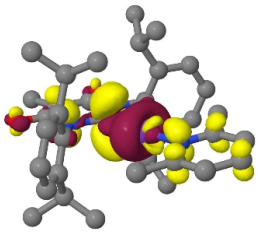

Figure S44. T2-S0 (MLCT(NHC)) difference density at the **2a** SLC-8.9 geometry.

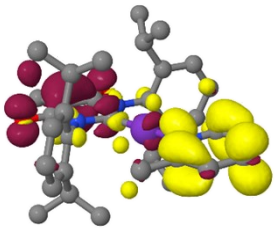

Figure S45. T3-S0 (LLCT) difference density at the **2a** SLC-8.9 geometry.

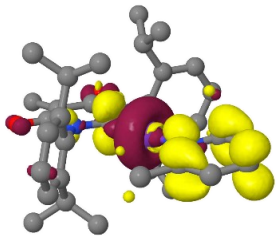

Figure S46. T9-S0 (MLCT) difference density at the **2a** SLC-8.9 geometry.

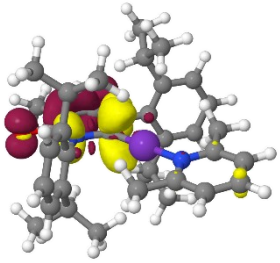

Figure S47. S1-S0 (LC(NHC)) difference density at the **2a** TLC geometry.

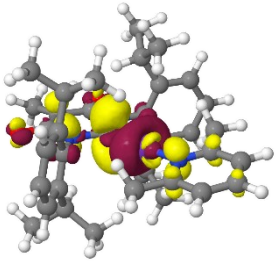

Figure S48. S2-S0 (MLCT(NHC)) difference density at the **2a** TLC geometry.

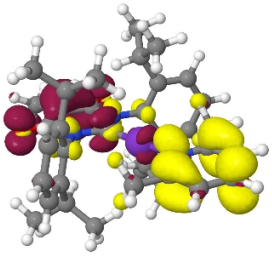

Figure S49. S3-S0 (LLCT) difference density at the **2a** TLC geometry.

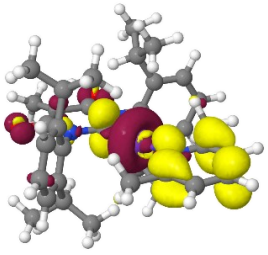

Figure S50. S5-S0 (MLCT) difference density at the **2a** TLC geometry.

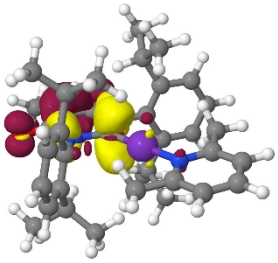

Figure S51. T1-S0 (LC(NHC)) difference density at the **2a** TLC geometry.

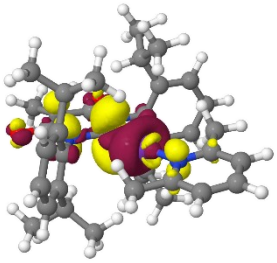

Figure S52. T2-S0 (MLCT(NHC)) difference density at the **2a** TLC geometry.

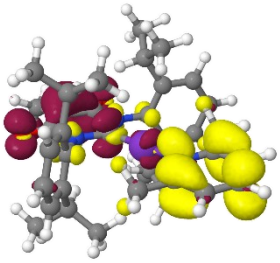

Figure S53. T3-S0 (LLCT) difference density at the **2a** TLC geometry.

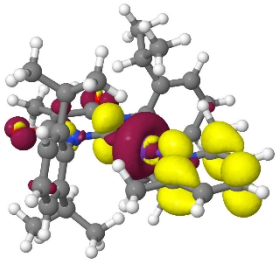

Figure S54. T9-S0 (MLCT) difference density at the **2a** TLC geometry.

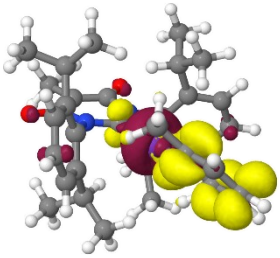

Figure S55. S1-S0 (MLCT) difference density at the **2a** SMLCT geometry.

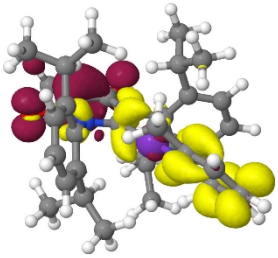

Figure S56. S2-S0 (LLCT) difference density at the **2a** SMLCT geometry.

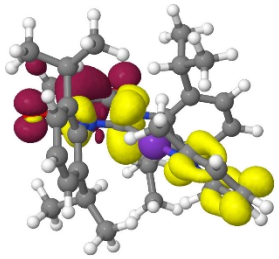

Figure S57. S3-S0 (LC(NHC)) difference density at the **2a** SMLCT geometry.

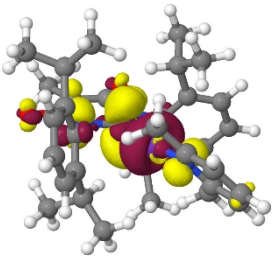

Figure S58. S4-S0 (MLCT(NHC)) difference density at the **2a** SMLCT geometry.

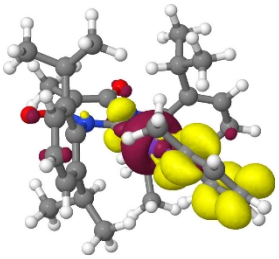

Figure S59. T1-S0 (MLCT) difference density at the **2a** SMLCT geometry.

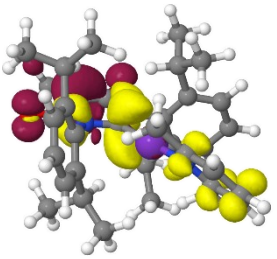

Figure S60. T2-S0 (LC(NHC)) difference density at the **2a** SMLCT geometry.

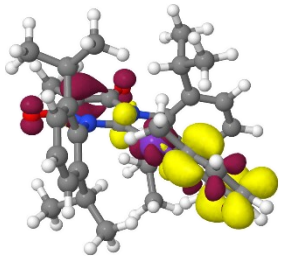

Figure S61. T3-S0 (LLCT) difference density at the **2a** SMLCT geometry.

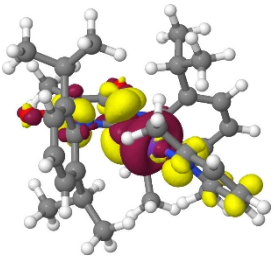

Figure S62. T5-S0 (MLCT(NHC)) difference density at the **2a** SMLCT geometry.

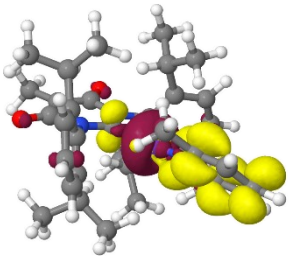

Figure S63. S1-S0 (MLCT) difference density at the **2a** TMLCT geometry.

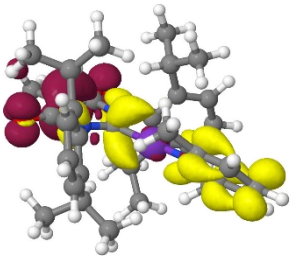

Figure S64. S2-S0 (LC/LLCT) difference density at the **2a** TMLCT geometry.

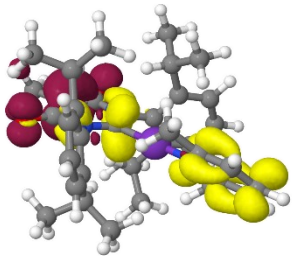

Figure S65. S3-S0 (LC/LLCT) difference density at the **2a** TMLCT geometry.

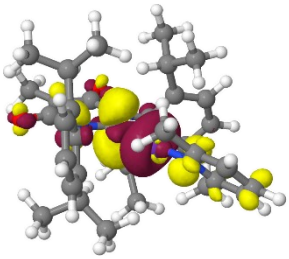

Figure S66. S4-S0 (MLCT(NHC)) difference density at the **2a** TMLCT geometry.

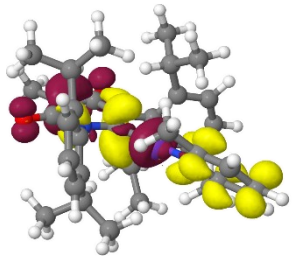

Figure S67. T1-S0 (LC/MLCT) difference density at the **2a** TMLCT geometry.

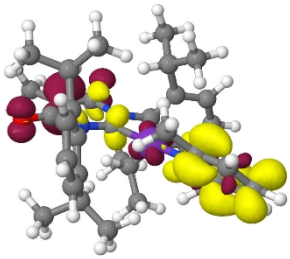

Figure S68. T4-S0 (LC/LLCT) difference density at the **2a** TMLCT geometry.

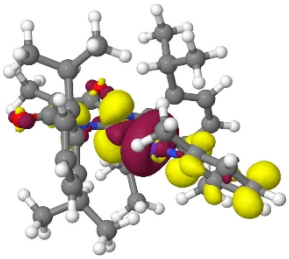

Figure S69. T5-S0 (MLCT(NHC)) difference density at the **2a** TMLCT geometry.

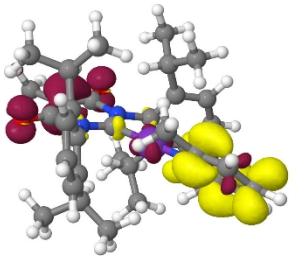

Figure S70. T9-S0 (LLCT) difference density at the **2a** TMLCT geometry.

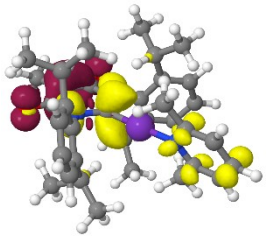

Figure S71. S1-S0 (LC) difference density at the **2a** TLLCT geometry.

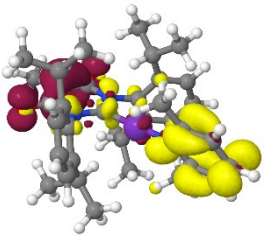

Figure S72. S2-S0 (LLCT) difference density at the **2a** TLLCT geometry.

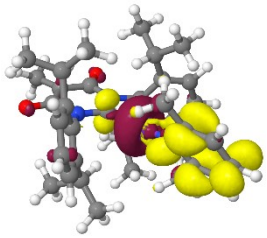

Figure S73. S3-S0 (MLCT) difference density at the **2a** TLLCT geometry.

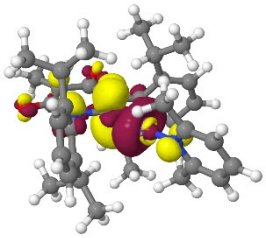

Figure S74. S4-S0 (MLCT(NHC)) difference density at the **2a** TLLCT geometry.

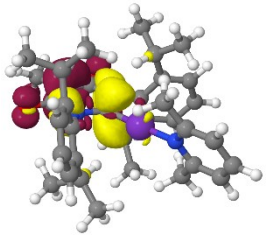

Figure S75. T1-S0 (LC) difference density at the **2a** TLLCT geometry.

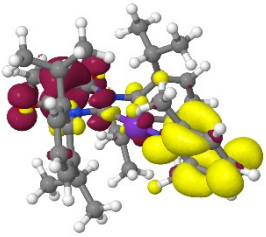

Figure S76. T2-S0 (LLCT) difference density at the **2a** TLLCT geometry.

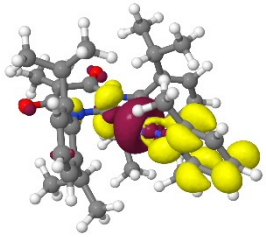

Figure S77. T3-S0 (MLCT) difference density at the **2a** TLLCT geometry.

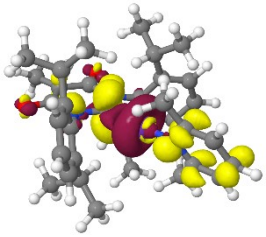

Figure S78. T4-S0 (MLCT(NHC)) difference density at the **2a** TLLCT geometry.

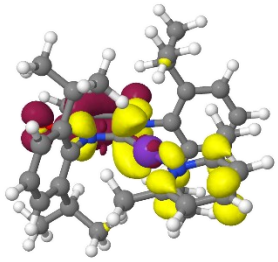

Figure S79. S1-S0 (LC/LLCT) difference density at the **2a** SLC/LLCT geometry.

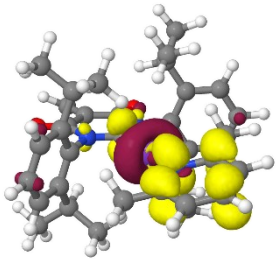

Figure S80. S2-S0 (MLCT) difference density at the **2a** SLC/LLCT geometry.

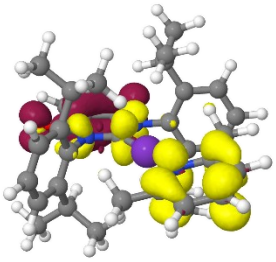

Figure S81. S3-S0 (LLCT/LC) difference density at the **2a** SLLCT/LC geometry.

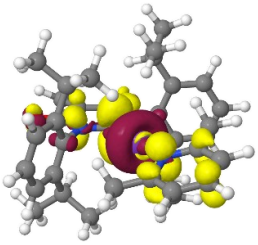

Figure S82. S4-S0 (MLCT(NHC)) difference density at the **2a** SLC/LLCT geometry.

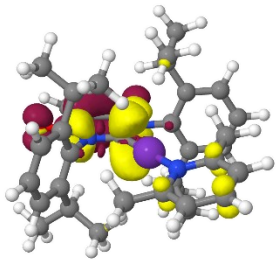

Figure S83. T1-S0 (LC) difference density at the **2a** SLC/LLCT geometry.

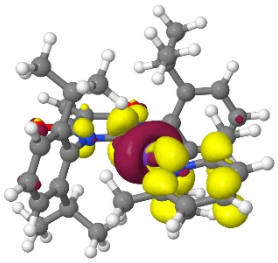

Figure S84. T2-S0 (MLCT) difference density at the **2a** SLC/LLCT geometry.

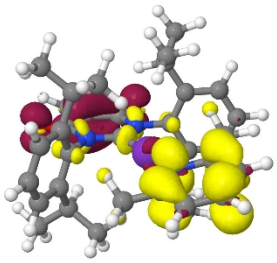

Figure S85. T3-S0 (LLCT) difference density at the **2a** SLC/LLCT geometry.

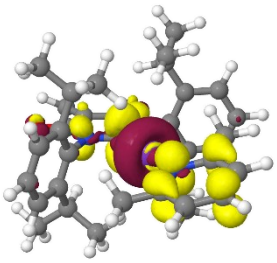

Figure S86. T9-S0 (MLCT(NHC)) difference density at the **2a** SLC/LLCT geometry.

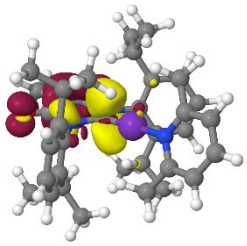

Figure S87. S1-S0 (LC) difference density at the **2a** SLC-65.6 geometry.

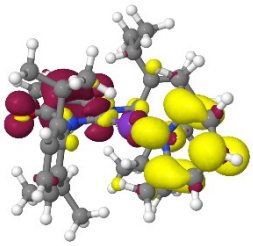

Figure S88. S2-S0 (LLCT) difference density at the **2a** SLC-65.6 geometry.

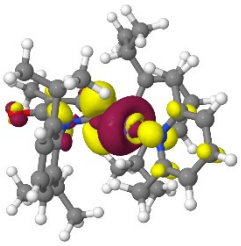

Figure S89. S3-S0 (MLCT(NHC)) difference density at the **2a** SLC-65.6 geometry.

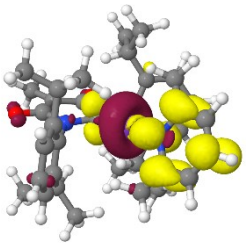

Figure S90. S4-S0 (MLCT) difference density at the **2a** SLC-65.6 geometry.

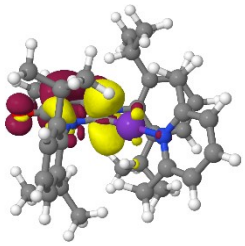

Figure S91. T1-S0 (LC) difference density at the **2a** SLC-65.6 geometry.

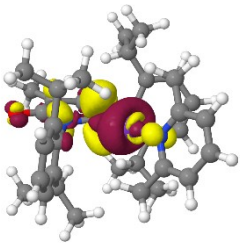

Figure S92. T2-S0 (MLCT(NHC)) difference density at the **2a** SLC-65.6geometry.

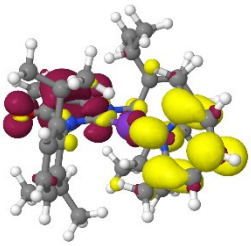

Figure S93. T3-S0 (LLCT) difference density at the **2a** SLC-65.6 geometry.

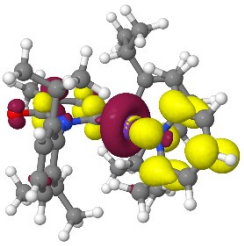

Figure S94. T4-S0 (MLCT) difference density at the **2a** SLC-65.6 geometry.

8.4. The linear formyl lutidine complex **2b**

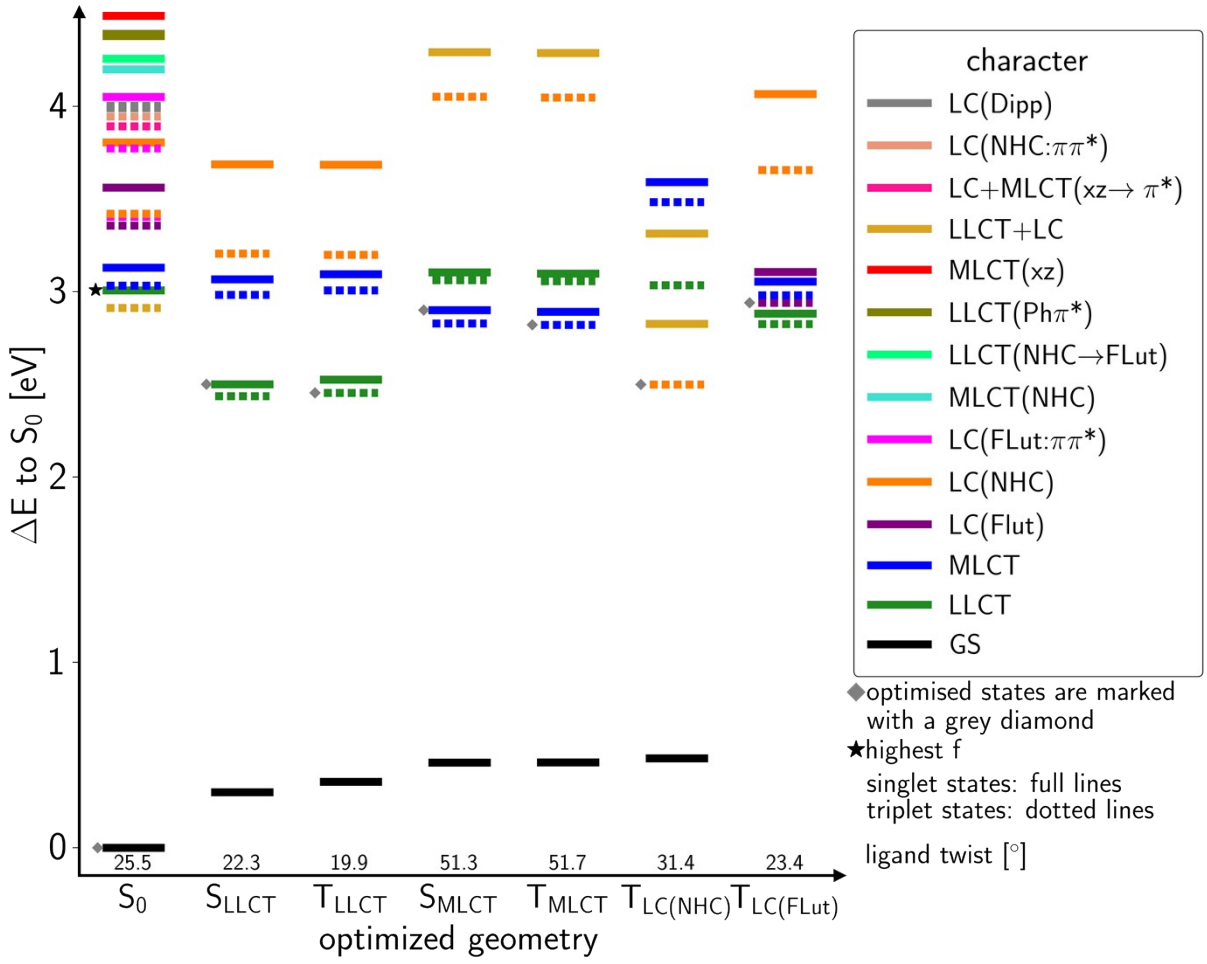

Figure S95. Energy state diagram of **2b** for selected optimized geometries.

Table S25. Singlet states and their properties at the ground state geometry of **2b**.

State	E [eV]	λ_{abs} [nm]	f	|μ| [D]	Character
S0	0			16.40	S0
S1	3.008	412	0.03057	16.47	LLCT
S2	3.130	396	0.00801	2.48	MLCT
S3	3.562	348	0	21.42	LC(FLut)
S4	3.815	326	0.08037	4.030	LC(NHC)
S5	4.051	306	0.0951	11.46	LC(FLut:ππ*)
S6	4.200	295	0.01486	18.55	MLCT(NHC)
S7	4.570	291	0.04309	4.65	LLCT
S8	4.380	283	0.02636	9.06	LLC(Phπ*)
S9	4.392	282	0.01382	13.36	LLC(Phπ*)
S10	4.489	276	0.07359	1.96	MLCT(xz)

Table S26. Triplet states and their properties at the ground state geometry of **2b**.

State	E [eV]	-	-	|μ| [D]	Character
T1	2.913			16.40	LLCT
T2	3.033			16.47	MLCT
T3	3.356			2.48	LC(FLut)
T4	3.404			21.42	LC(FLut:ππ*)
T5	3.421			4.03	LC(NHC)
T6	3.773			11.46	LC(FLut:ππ*)
T7	3.893			18.55	MLCT(NHC)
T8	3.945			4.65	LC(NHC:ππ*)
T9	3.991			9.06	LC(Dipp)
T10	4.004			13.36	LC(Dipp)

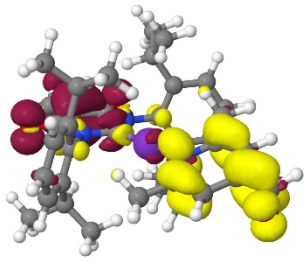

Figure S96. S1-S0 difference density at the GS of **2b**.

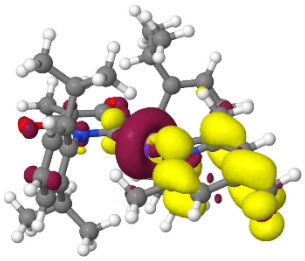

Figure S97. S2-S0 difference density at the GS of **2b**.

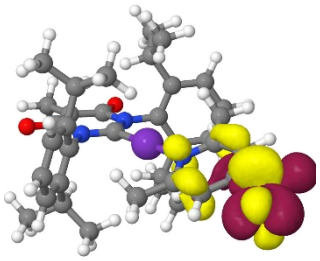

Figure S98. S3-S0 difference density at the GS of **2b**.

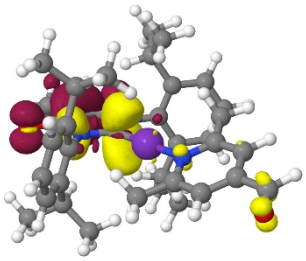

Figure S99. S4-S0 difference density at the GS of **2b**.

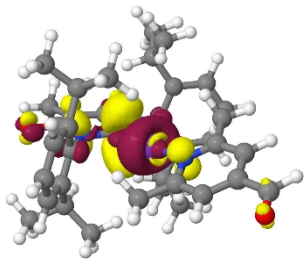

Figure S100. S5-S0 difference density at the GS of **2b**.

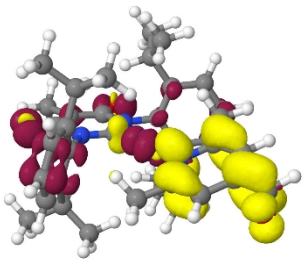

Figure S101. S6-S0 difference density at the GS of **2b**.

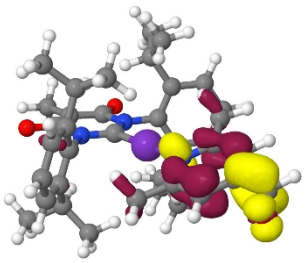

Figure S102. S7-S0 difference density at the GS of **2b**.

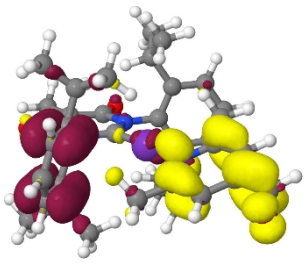

Figure S103. S8-S0 difference density at the GS of **2b**.

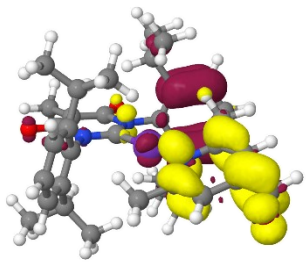

Figure S104. S9-S0 difference density at the GS of **2b**.

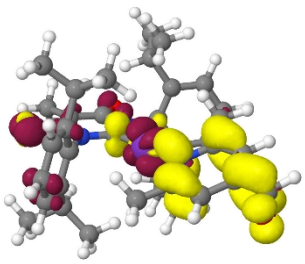

Figure S105. S10-S0 difference density at the GS of **2b**.

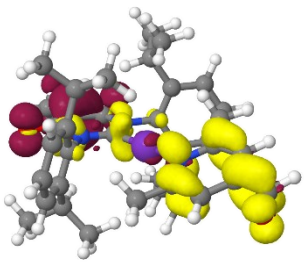

Figure S106. T1-S0 difference density at the GS of **2b**.

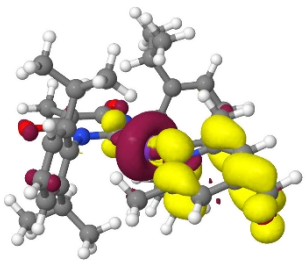

Figure S107. T2-S0 difference density at the GS of **2b**.

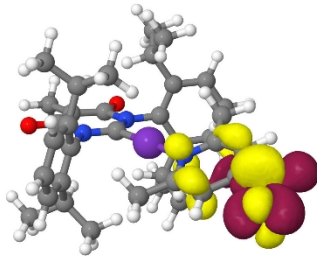

Figure S108. T3-S0 difference density at the GS of **2b**.

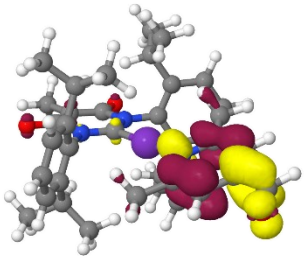

Figure S109. T4-S0 difference density at the GS of **2b**.

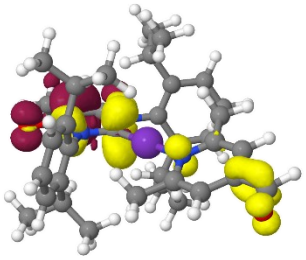

Figure S110. T5-S0 difference density at the GS of **2b**.

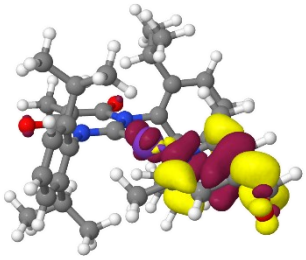

Figure S111. T6-S0 difference density at the GS of **2b**.

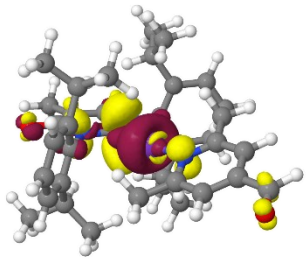

Figure S112. T7-S0 difference density at the GS of **2b**.

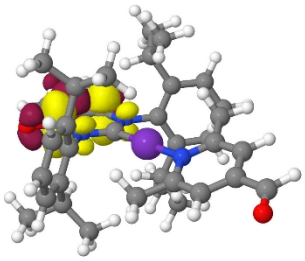

Figure S113. T8-S0 difference density at the GS of **2b**.

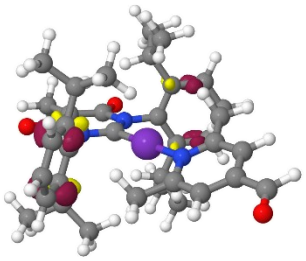

Figure S114. T9-S0 difference density at the GS of **2b**.

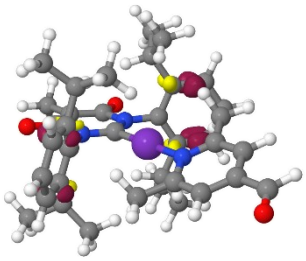

Figure S115. T10-S0 difference density at the GS of **2b**.

Table S27. Energies [eV] of relevant excited states of **2b** at the optimized geometries of different states.

State	Optimized geometry						
	S0	SLLCT	TLLCT	SMLCT	TMLCT	TLC(NHC)	TLC(FLut)
S0	0.000	0.300	0.355	0.459	0.460	0.482	0.303
SLLCT	3.008	2.500	2.525	3.104	3.098	2.827	2.882
TLLCT	2.913	2.436	2.454	3.062	3.057	3.035	2.825
SMLCT	3.130	3.067	3.094	2.900	2.892	3.592	3.055
TMLCT	3.033	2.437	3.008	2.829	2.821	3.484	2.981
TLC	4.380	3.206	3.199	4.052	4.048	2.499	3.657
Tnπ	3.357	3.217	3.267	3.328	3.330	3.713	2.940

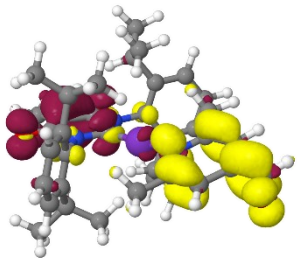

Figure S116. S1-S0 (LLCT) difference density at the **2b** SLLCT geometry.

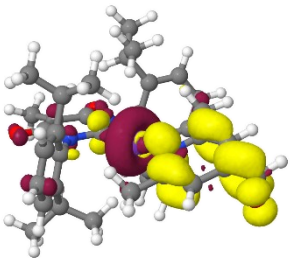

Figure S117. S2-S0 (MLCT) difference density at the **2b** SLLCT geometry.

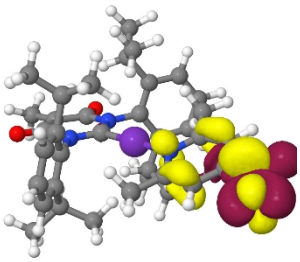

Figure S118. S3-S0 (LC(FLut)) difference density at the 2b SLLCT geometry.

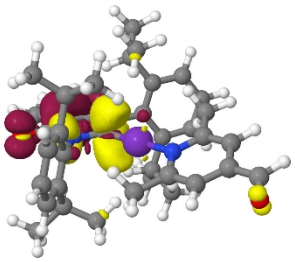

Figure S119. S4-S0 (LC(NHC)) difference density at the 2b SLLCT geometry.

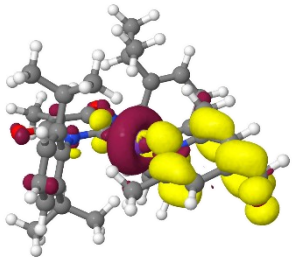

Figure S120. T1-S0 (LLCT) difference density at the **2b** SLLCT geometry.

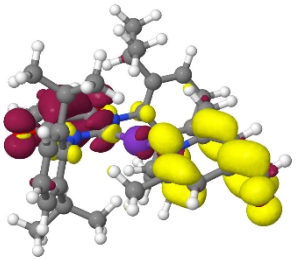

Figure S121. T2-S0 (MLCT) difference density at the **2b** SLLCT geometry.

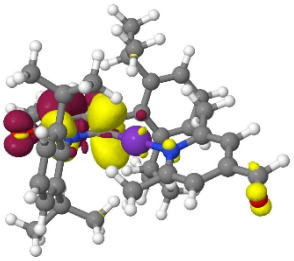

Figure S122. T3-S0 (LC(NHC)) difference density at the **2b** SLLCT geometry.

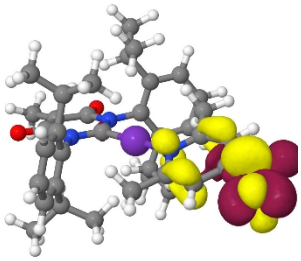

Figure S123.T4-S0 (LC(FLut)) difference density at the **2b** SLLCT geometry.

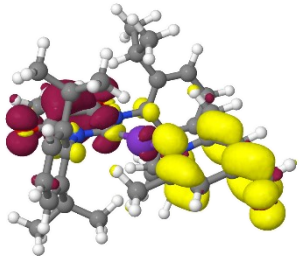

Figure S124. S1-S0 (LLCT) difference density at the **2b** TLLCT geometry.

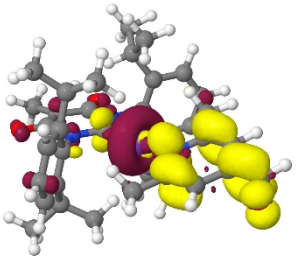

Figure S125. S2-S0 (MLCT) difference density at the **2b** TLLCT geometry.

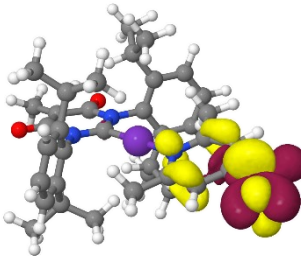

Figure S126. S3-S0 (LC(FLut)) difference density at the **2b** TLLCT geometry.

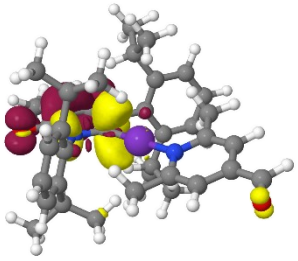

Figure S127. S4-S0 (LC(NHC)) difference density at the **2b** TLLCT geometry.

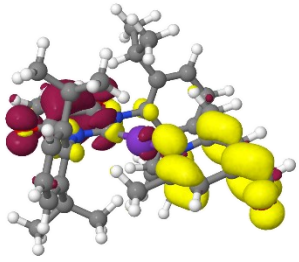

Figure S128. T1-S0 (LLCT) difference density at the **2b** TLLCT geometry.

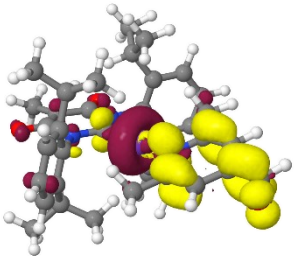

Figure S129. T2-S0 (MLCT) difference density at the **2b** TLLCT geometry.

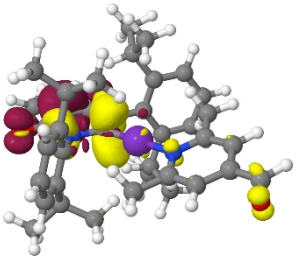

Figure S130. T3-S0 (LC(NHC)) difference density at the **2b** TLLCT geometry.

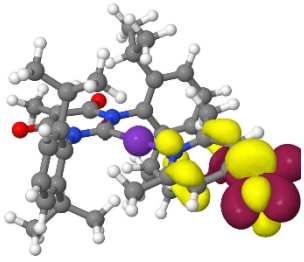

Figure S131. T4-S0 (LC(FLut)) difference density at the **2b** TLLCT geometry.

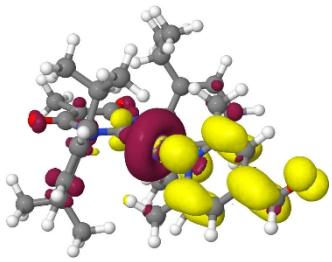

Figure S132. S1-S0 (MLCT) difference density at the **2b** SMLCT geometry.

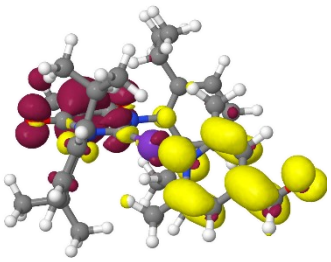

Figure S133. S2-S0 (LLCT) difference density at the **2b** SMLCT geometry.

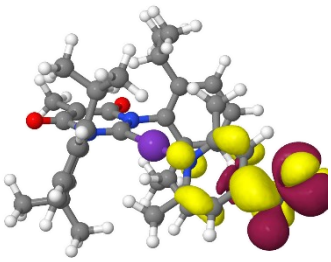

Figure S134. S3-S0 (LC(FLut)) difference density at the **2b** SMLCT geometry.

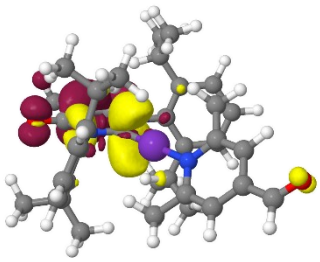

Figure S 135. S9-S0 (LC(NHC)) difference density at the **2b** SMLCT geometry.

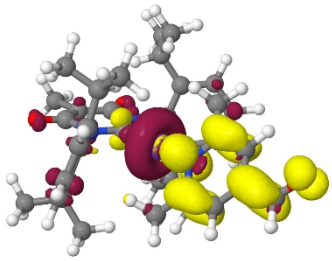

Figure S136. T1-S0 (MLCT) difference density at the **2b** SMLCT geometry.

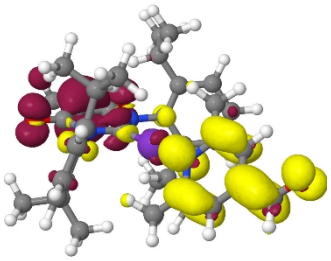

Figure S137. T2-S0 (LLCT) difference density at the **2b** SMLCT geometry.

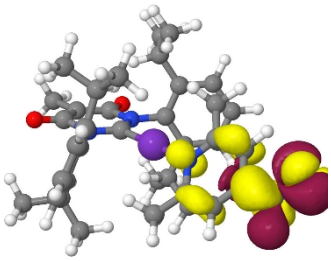

Figure S138. T3-S0 (LC(FLut)) difference density at the **2b** SMLCT geometry.

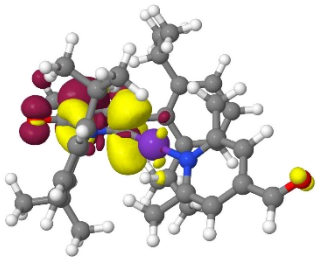

Figure S139. T6-S0 (LC(NHC)) difference density at the **2b** SMLCT geometry.

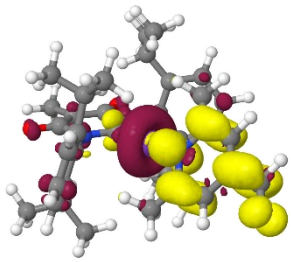

Figure S140. S1-S0 (MLCT) difference density at the **2b** TMLCT geometry.

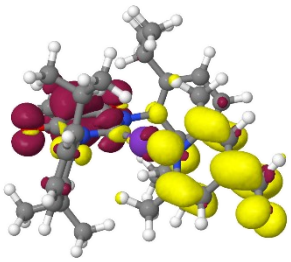

Figure S141. S2-S0 (LLCT) difference density at the **2b** TMLCT geometry.

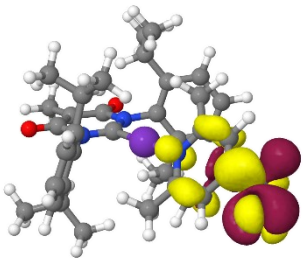

Figure S142. S3-S0 (FLut) difference density at the **2b** TMLCT geometry.

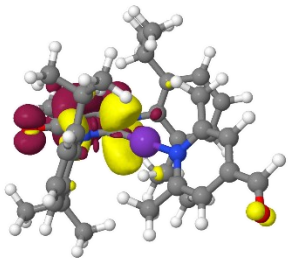

Figure S143. S9-S0 (LC(NHC)) difference density at the **2b** TMLCT geometry.

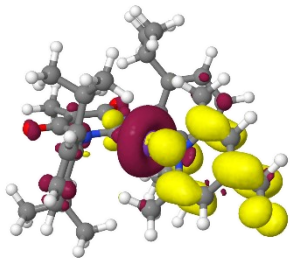

Figure S144. T1-S0 (MLCT) difference density at the **2b** TMLCT geometry.

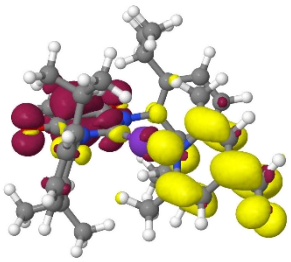

Figure S145. T2-S0 (LLCT) difference density at the **2b** TMLCT geometry.

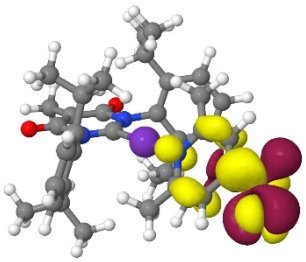

Figure S146. T3-S0 (LC(FLut)) difference density at the **2b** TMLCT geometry.

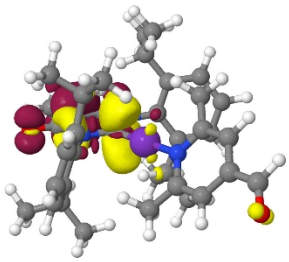

Figure S147. T6-S0 (LC(NHC)) difference density at the **2b** TMLCT geometry.

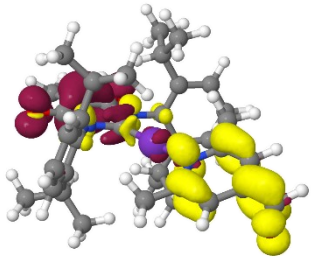

Figure S148. S1-S0 (LLCT) difference density at the **2b** TLC(NHC) geometry.

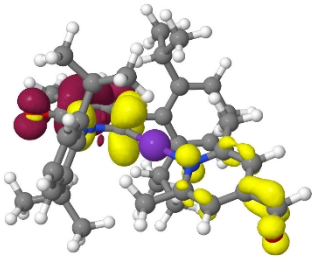

Figure S149. S2-S0 (LC(NHC)) difference density at the **2b** TLC(NHC) geometry.

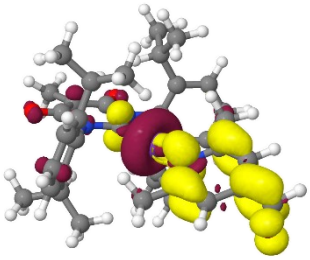

Figure S150. S3-S0 (MLCT) difference density at the **2b** TLC(NHC) geometry.

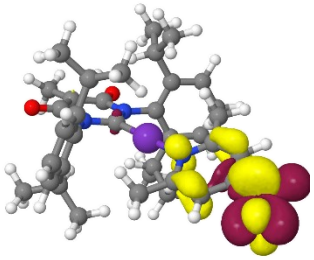

Figure S151. S1-S0 (LC(FLut)) difference density at the **2b** TLC(NHC) geometry.

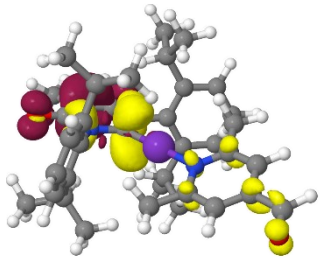

Figure S152. T1-S0 (LLCT) difference density at the **2b** TLC(NHC) geometry.

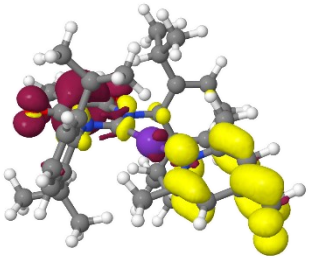

Figure S153. T2-S0 (LLCT) difference density at the **2b** TLC(NHC) geometry.

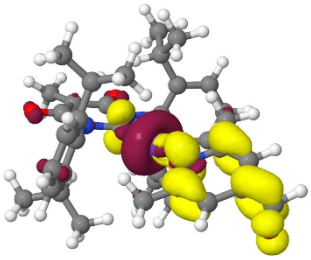

Figure S154. T3-S0 (MLCT) difference density at the **2b** TLC(NHC) geometry.

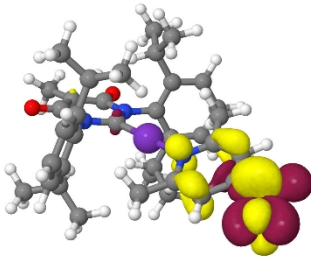

Figure S155. T4-S0 (LC(FLut)) difference density at the **2b** TLC(NHC) geometry.

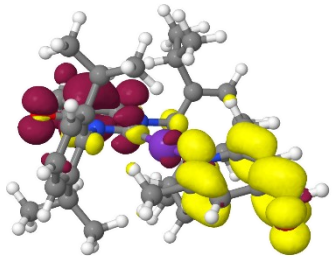

Figure S156. S4-S0 (LLCT) difference density at the **2b** TLC(FLut) geometry.

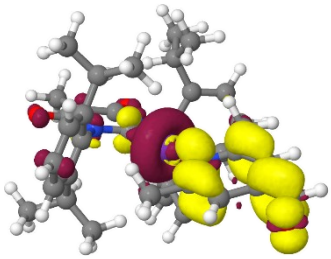

Figure S157. S4-S0 (MLCT) difference density at the **2b** TLC(FLut) geometry.

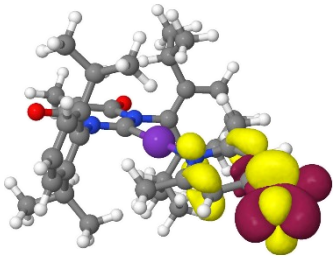

Figure S158. S4-S0 (LC(FLut)) difference density at the **2b** TLC(FLut) geometry.

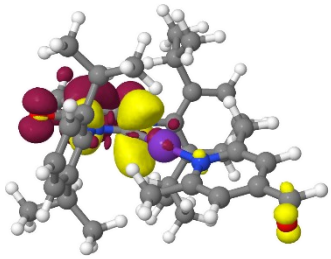

Figure S159. S4-S0 (LC(NHC)) difference density at the **2b** TLC(FLut) geometry.

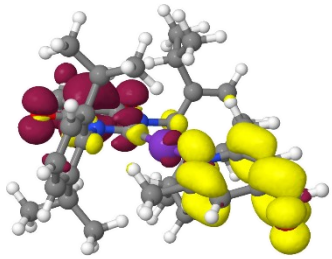

Figure S160. T1-S0 (LLCT) difference density at the **2b** TLC(FLut) geometry.

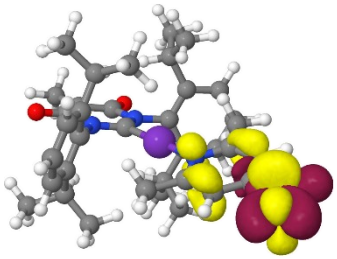

Figure S161. T2-S0 (LC(FLut)) difference density at the **2b** TLC(FLut) geometry.

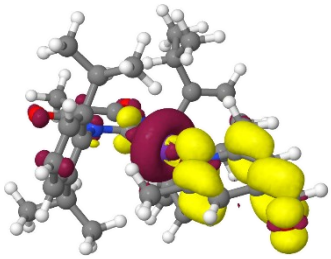

Figure S162. T3-S0 (MLCT) difference density at the **2b** TLC(FLut) geometry.

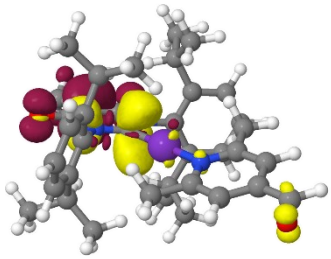

Figure S163. T4-S0 (LC(NHC)) difference density at the **2b** TLC(FLut) geometry.

8.4.1. MLCT/LLCT interconversion in **2b**

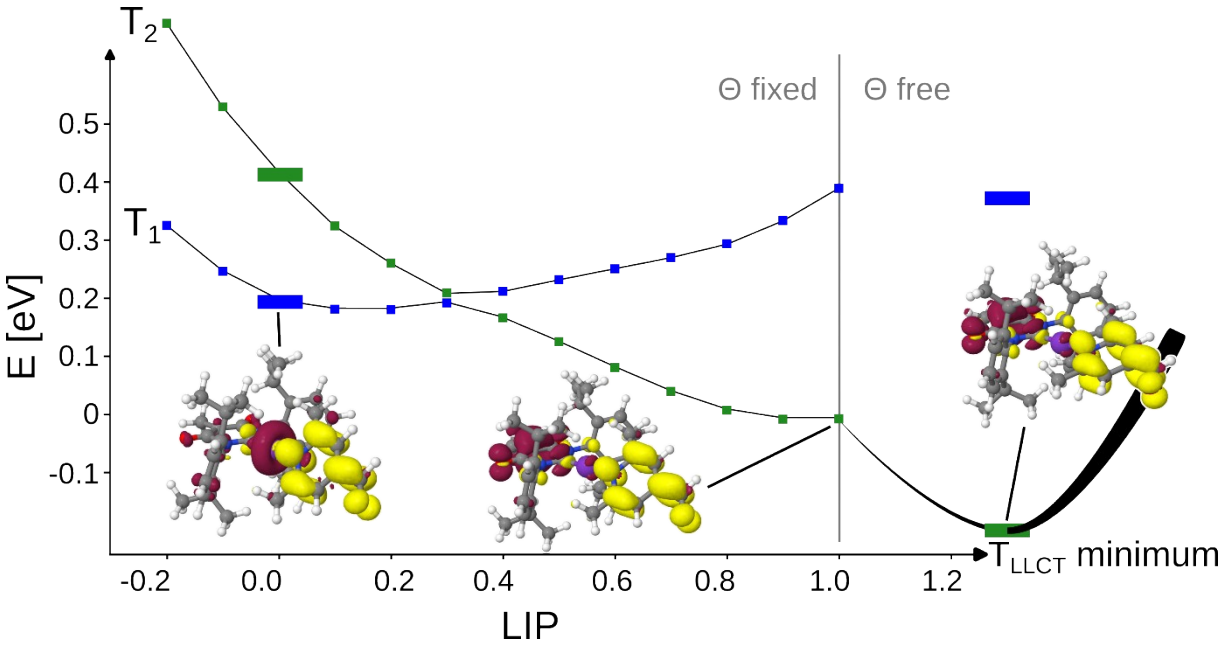

Figure S 164. Linear interpolation in-between the freely optimised T_{MLCT} minimum (Θ=51.3 °) (0.0) and constrained optimised T_{LLCT}, for which the torsion angle was fixed to 51.3°(1.0). The energy barrier towards this constrained minimum is 12 meV. A free geometry optimisation starting from the constrained optimised T_{LLCT} state leads to the structure of the T_{LLCT} minimum.

8.5. The trigonal pyridine complex **3a**

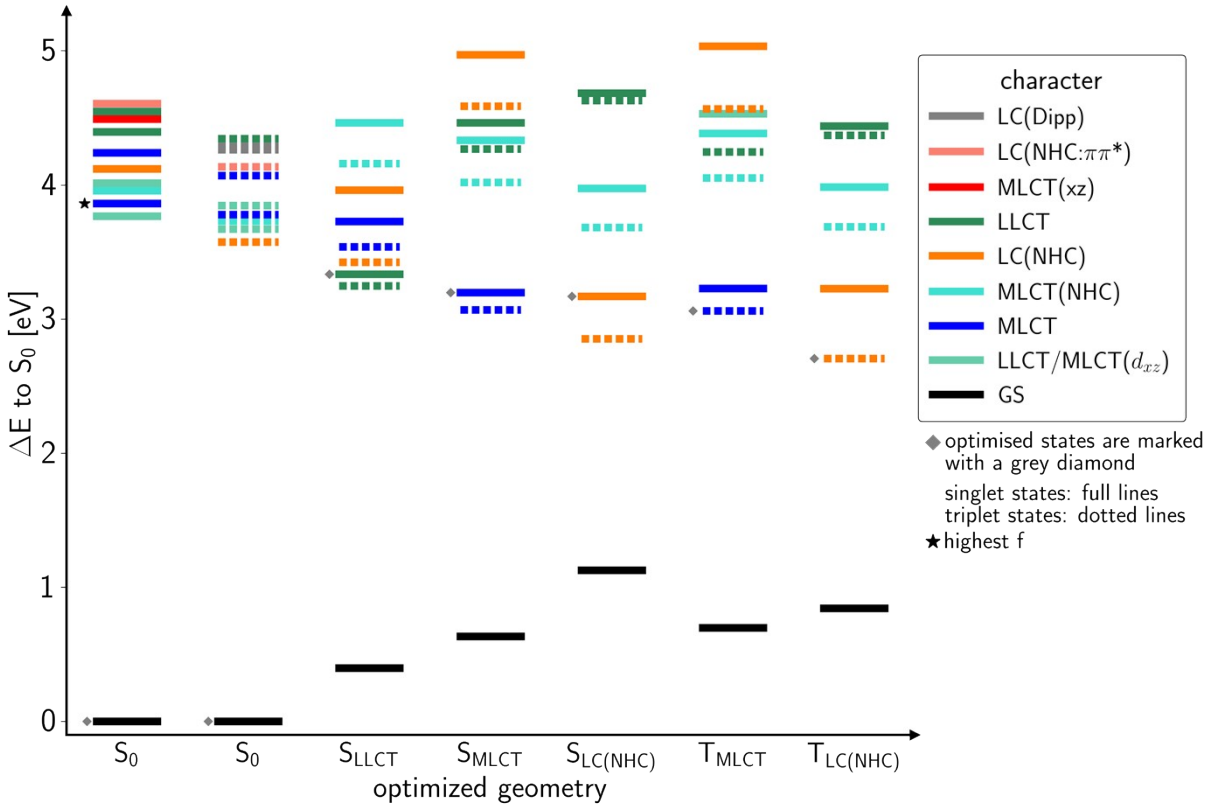

Figure S165. Energy state diagram of **3a** for selected optimized geometries.

Table S28. Singlet states and their properties at the ground state geometry of **3a**.

State	E [eV]	λ_{abs} [nm]	f	|μ| [D]	Character
S0	0			23.01	S0
S1	3.767	329	0.00916	9.41	LLCT/MLCT(xz)
S2	3.862	321	0.14889	12.74	MLCT
S3	3.957	313	0.05833	21.73	MLCT(NHC)
S4	4.014	309	0.08989	10.29	LLCT/MLCT(xz)
S5	4.120	301	0.02919	13.10	LC(NHC)
S6	4.241	292	0.01188	18.09	MLCT
S7	4.395	282	0.00707	0.49	LLCT
S8	4.491	276	0.00007	8.07	MLCT(dxz)
S9	4.555	273	0.01124	3.71	LLCT
S10	4.606	269	0.00258	12.72	LC(NHC:ππ*)

Table S29. Triplet states and their properties at the ground state geometry of **3a**.

State	E [eV]			|μ| [D]	Character
T1	3.574			23.01	LC(NHC)
T2	3.671			9.41	LLCT/MLCT(dxz)
T3	3.731			12.74	MLCT(NHC)
T4	3.778			21.73	MLCT
T5	3.846			10.29	LLCT/MLCT(dxz)
T6	4.070			13.10	MLCT
T7	4.135			18.09	LC(NHC:ππ*)
T8	4.263			0.49	LC(Dipp)
T9	4.287			8.07	LC(Dipp)
T10	4.344			3.71	LLCT

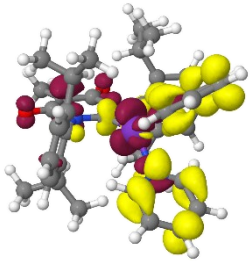

Figure S166. S1 difference density at the GS of **3a**.

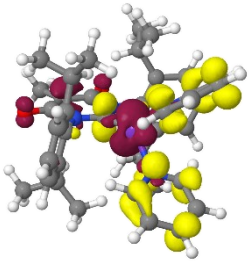

Figure S167. S2 difference density at the GS of **3a**.

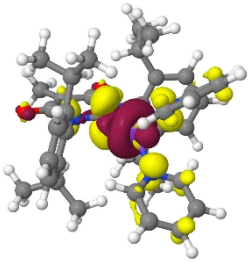

Figure S168. S3 difference density at the GS of **3a**.

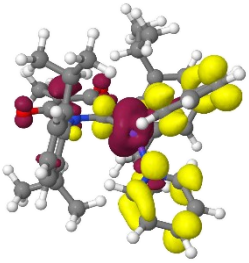

Figure S169. S4 difference density at the GS of **3a**.

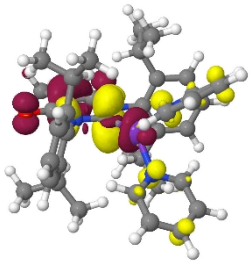

Figure S170. S5 difference density at the GS of **3a**.

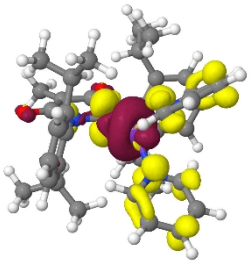

Figure S171. S6 difference density at the GS of **3a**.

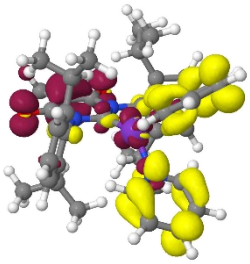

Figure S172. S7 difference density at the GS of **3a**.

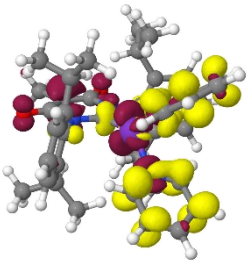

Figure S173. S8 difference density at the GS of **3a**.

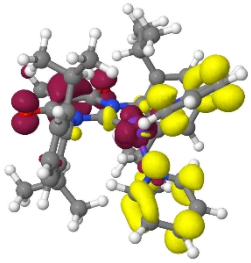

Figure S174. S9 difference density at the GS of **3a**.

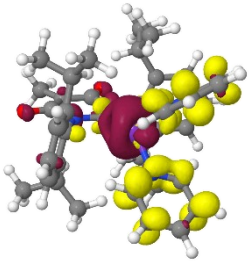

Figure S175. S10 difference density at the GS of **3a**.

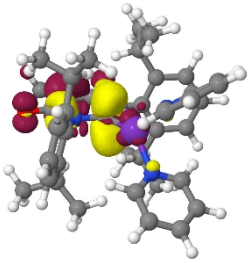

Figure S176. T1 difference density at the GS of **3a**.

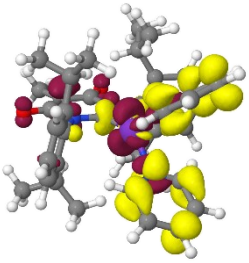

Figure S177. T2 difference density at the GS of **3a**.

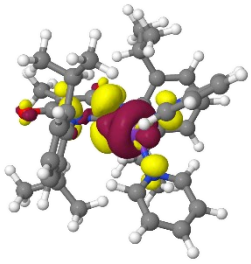

Figure S178. T3 difference density at the GS of **3a**.

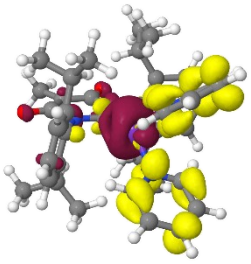

Figure S179. T4 difference density at the GS of **3a**.

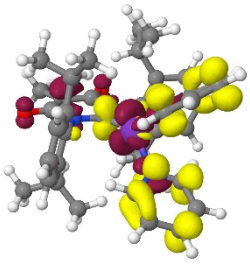

Figure S180. T5 difference density at the GS of **3a**.

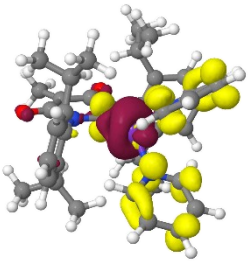

Figure S181. T6 difference density at the GS of **3a**.

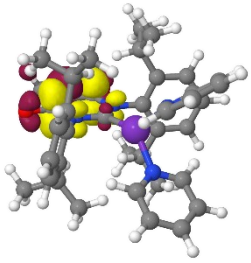

Figure S182. T7 difference density at the GS of **3a**.

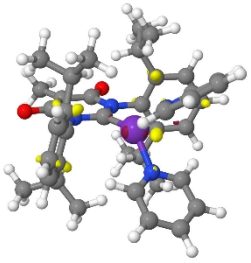

Figure S183. T8 difference density at the GS of **3a**.

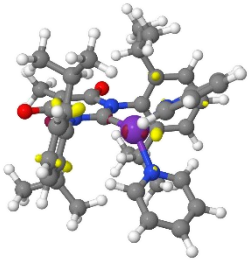

Figure S184. T9 difference density at the GS of **3a**.

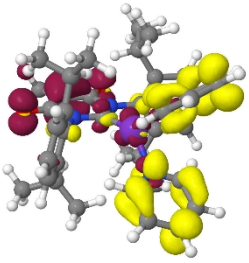

Figure S185. T10 difference density at the GS of **3a**.

Table S30. Energies [eV] of relevant excited states of **3a** at the optimized geometries of different states.

State	Optimized geometry					
	S0	SLLCT	SMLCT	TMLCT	SLC	TLC
S0	0.000	0.398	0.634	0.698	1.127	0.843
SLLCT	3.767	3.335	4.451	4.531	4.685	4.438
TLLCT	3.574	3.247	4.228	4.2459	4.630	4.438
SMLCT	3.862	3.728	3.197	3.228	-	-
TMLCT	3.778	3.538	3.068	3.061	-	-
SLC	3.862	3.960	4.950	5.034	3.170	3.227
TLC	3.574	3.424	4.557	4.567	2.853	2.706
SMLCT(NHC)	3.957	4.463	4.317	4.383	3.975	3.984
TMLCT(NHC)	3.731	4.159	3.977	4.052	3.683	3.688

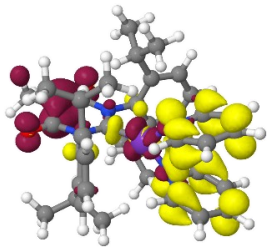

Figure S186. S1-S0 (LLCT) difference density at the **3a** SLLCT geometry.

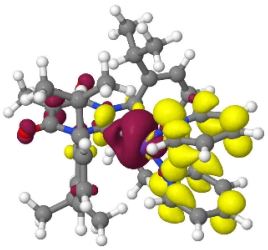

Figure S187. S2-S0 (MLCT) difference density at the **3a** SLLCT geometry.

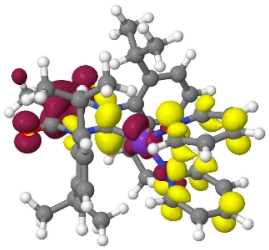

Figure S188. S4-S0 (LC(NHC)) difference density at the **3a** SLLCT geometry.

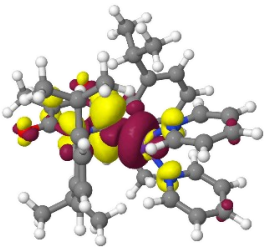

Figure S189. S7-S0 (MLCT(NHC)) difference density at the **3a** SLLCT geometry.

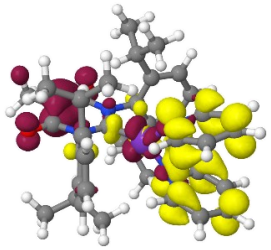

Figure S190. T1-S0 (LLCT) difference density at the **3a** SLLCT geometry.

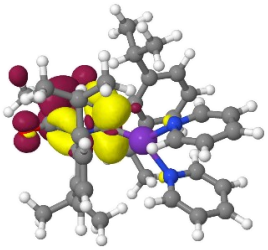

Figure S191. T2-S0 (LC(NHC)) difference density at the **3a** SLLCT geometry.

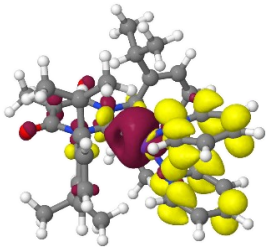

Figure S192. T3-S0 (MLCT) difference density at the **3a** SLLCT geometry.

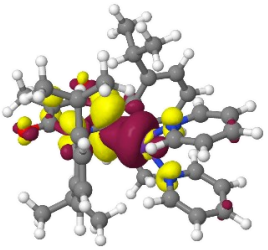

Figure S193. T5-S0 (MLCT(NHC)) difference density at the **3a** SLLCT geometry.

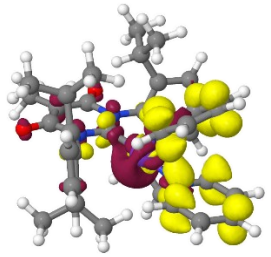

Figure S194. S1-S0 (MLCT) difference density at the **3a** SMLCT geometry.

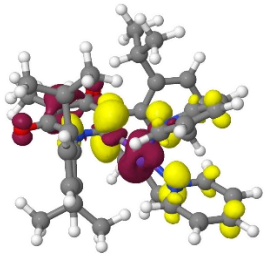

Figure S195. S4-S0 (MLCT(NHC)) difference density at the **3a** SMLCT geometry.

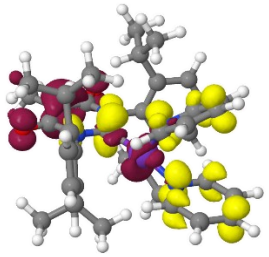

Figure S196. S5-S0 (LLCT) difference density at the **3a** SMLCT geometry.

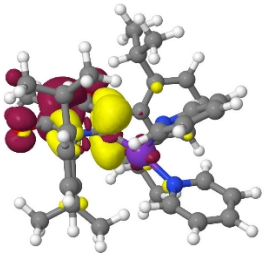

Figure S197. S9-S0 (LC(NHC)) difference density at the **3a** SMLCT geometry.

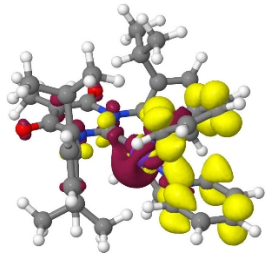

Figure S198. T1-S0 (MLCT) difference density at the **3a** SMLCT geometry.

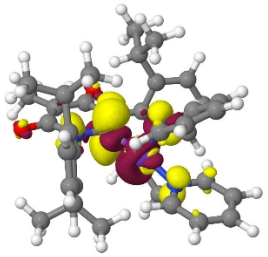

Figure S199. T3-S0 (MLCT(NHC)) difference density at the **3a** SMLCT geometry.

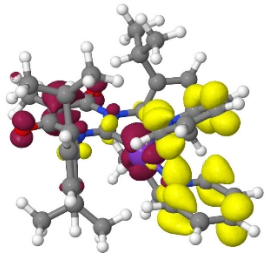

Figure S200. T5-S0 (LLCT) difference density at the **3a** SMLCT geometry.

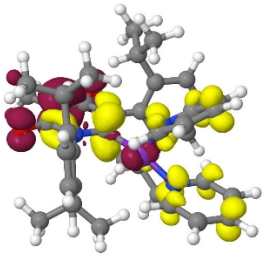

Figure S201. T7-S0 (LC(NHC)) difference density at the **3a** SMLCT geometry.

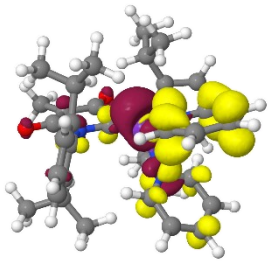

Figure S202. S1-S0 (MLCT) difference density at the **3a** TMLCT geometry.

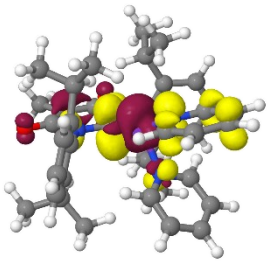

Figure S203. S4-S0 (MLCT(NHC)) difference density at the **3a** TMLCT geometry.

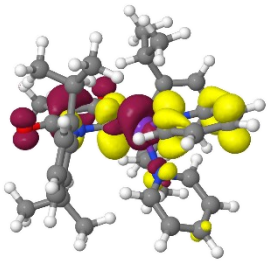

Figure S204. S5-S0 (LLCT) difference density at the **3a** TMLCT geometry.

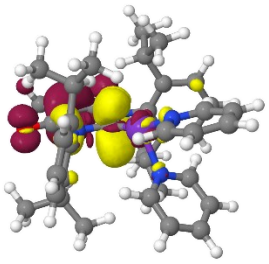

Figure S205. S9-S0 (LC(NHC)) difference density at the **3a** TMLCT geometry.

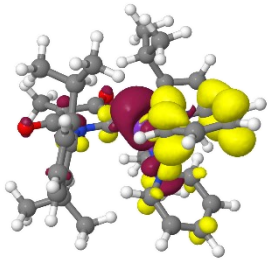

Figure S206. T2-S0 (MLCT) difference density at the **3a** TMLCT geometry.

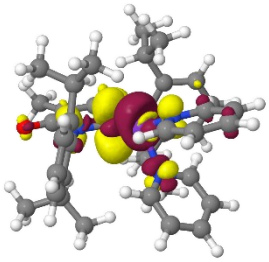

Figure S207. T3-S0 (MLCT(NHC)) difference density at the **3a** TMLCT geometry.

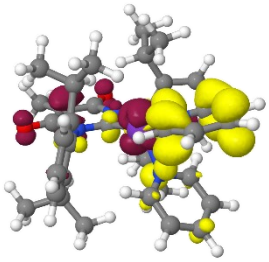

Figure S208. T5-S0 (LLCT) difference density at the **3a** TMLCT geometry.

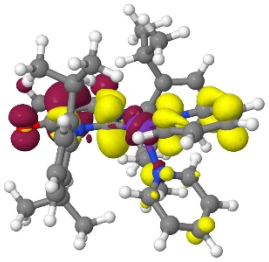

Figure S209. T6-S0 (LC(NHC)) difference density at the **3a** TMLCT geometry.

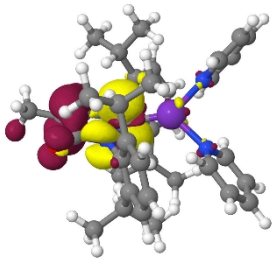

Figure S210. S1-S0 (LC(NHC)) difference density at the **3a** SLC(NHC) geometry.

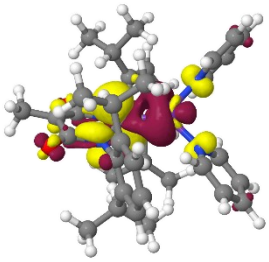

Figure S211. S2-S0 (MLCT(NHC)) difference density at the **3a** SLC(NHC) geometry.

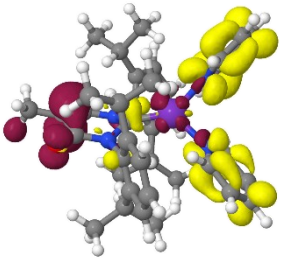

Figure S212. S4-S0 (LLCT) difference density at the **3a** SLC(NHC) geometry.

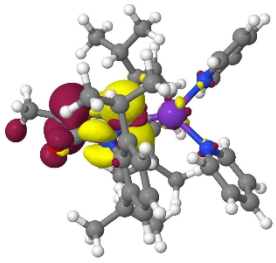

Figure S213. S1-S0 (LC(NHC)) difference density at the **3a** SLC(NHC) geometry.

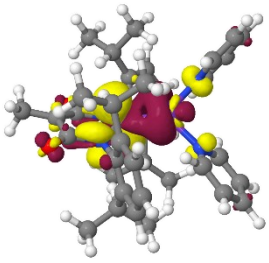

Figure S214. S2-S0 (MLCT(NHC)) difference density at the **3a** SLC(NHC) geometry.

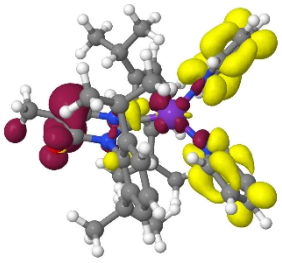

Figure S215. S4-S0 (LLCT) difference density at the **3a** SLC(NHC) geometry.

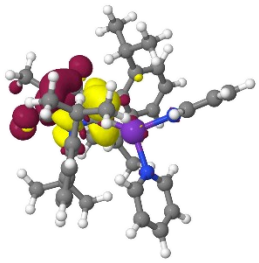

Figure S216. S1-S0 (LC(NHC)) difference density at the **3a** TLC(NHC) geometry.

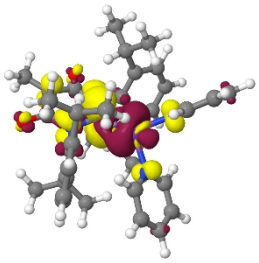

Figure S217. S2-S0 (MLCT) difference density at the **3a** TLC(NHC) geometry.

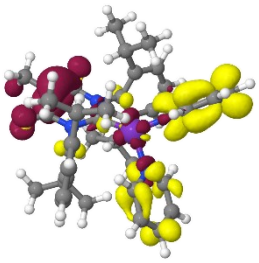

Figure S218. S4-S0 (LLCT) difference density at the **3a** TLC(NHC) geometry.

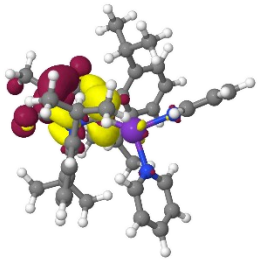

Figure S219. T1-S0 (LC(NHC)) difference density at the **3a** TLC(NHC) geometry.

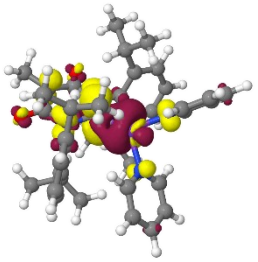

Figure S220. T2-S0 (MLCT(NHC)) difference density at the **3a** TLC(NHC) geometry.

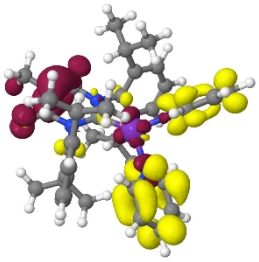

Figure S221. T5-S0 (LLCT) difference density at the **3a** TLC(NHC) geometry.

8.5.1. State interconversion in **3a**

For many pairs of states, vibrational, a vibrational overlap could not be calculated in harmonic approximation due to the large difference in structure. The sum of the $SOCME^2$ values permit an idea of the transition strengths in-between the states.

Table S31. $SOCME^2$ values [cm^{-2}] in-between the optimized state to other low-lying excited states in **3a**. No MLCT(d_{z2}) was found at the optimized geometries of the S_{LC} and T_{LC} states.

State	Optimized geometry				
	SLLCT	SMLCT	SLC	TMLCT	TLC
LLCT	99.2	137268	1721.8	15322.4	1106.9
MLCT	95483.8	282.3	-	2112	-
LC	107.2	4055.5	10.8	2218.2	1.5

8.5.2. T1-absorption in **3a**

Experimentally, the emission spectra were obtained while exciting at 375 nm. The first excited singlet state lies at 329 nm and is not very bright (f = 0.00916). The first triplet state is a T_{LC} at 349 nm. Due to intensity borrowing, which is elaborated below, the first triplet state possesses a non-zero oscillator strengths. Light at 375 nm could thus only excite the first triplet.

The T_{LC} consists of a sizeable admixture of a MLCT from the d_{z^2}-orbital to the antibonding carbene orbital. It can be expected, that this contribution is the major component of the (S_0-T_1) transition dipole moment.

Table S32. Admixture coefficients of the bright T_{LC} substate and transition dipole moment components of the S_n state and the T_{LC} state with the S_0 state at different geometries for **3a**.

opt. geo	Coupled state	SOCME (H_x, H_y, H_z) [cm^{-1}] $\langle T_{LC} \vert \hat{H}_{SO} \vert S_n \rangle$	admixture coeff.	$\mu(S_n\text{-}S_0)$-component [ea_0]		
				x	y	z
T_{LC}	S_2: MLCT(NHC)	31, -101, 13	0.01009	0.43358	-0.01796	-0.02132
T_{LC}	Total $\mu(T_{LC}\text{-}S_0)$			-0.00468	-0.00085	-0.00400
S_0	S_3: MLCT(NHC)	40, -196, 33	0.06505	0.77498	-0.01337	-0.29250
S_0	S_1: LLCT	5, -24, 4	0.01662	-0.30765	-0.05540	0.03992
S_0	Total $\mu(T_{LC}\text{-}S_0)$			-0.04855	-0.00037	0.00000

The different admixture strength may be caused by the different energy difference:

Table S33. Energy differences in **3a**.

States @ opt geo	T_1-S_3 @ S0	T_1-S_1 @ S0	T_1-S_2 @ TLC
ΔE [eV]	0.384	0.1936	1.245

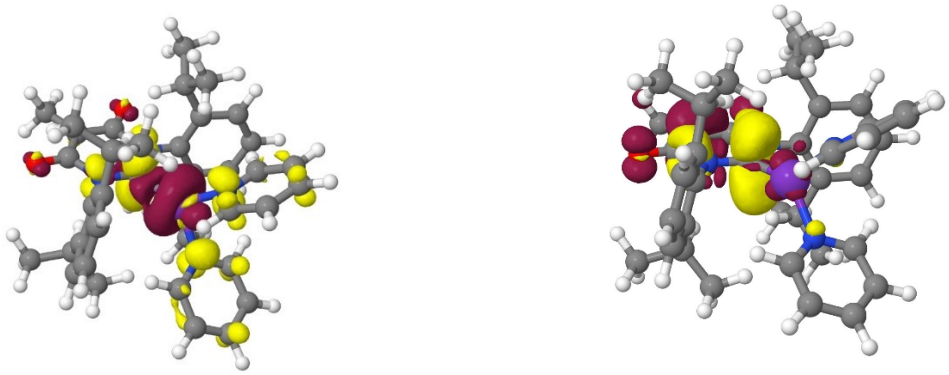

Figure S222. Difference densities of the S_3 @ S0 (left) and the T_1 @ S0 (right).

Figure S 223. Difference densities of the S_3 @ T_{LC} (left) and the T_1 @ T_{LC} (right).

The comparison towards the Lutidine-bearing complex **2a** can be drawn. In **2a**, the MLCT(NHC) has a non-zero transition dipole moment to the S_0 as-well. It seems, that the S_{MLCT}-admixture is however not sufficient to facilitate a sizeable transition dipole moment to the GS.

Table S34. Admixture coefficients towards the T_{LC} and transition dipole moment components of the S_n and the T_{LC} with the S_0 at different geometries for **2a**.

opt. geo	Coupled state	Σ SOCME^2 [cm^{-2}] $\langle T_{LC} \vert \hat{H}_{SO} \vert S_0 \rangle$	admixture coeff.	μ(S_n-S_0)-component [ea_0]		
				x	x	x
T_{LC}	S_2: MLCT(NHC)	3609	0.00444	0.47254	-0.00257	-0.07628
T_{LC}	Total μ(T_{LC}-S_0)			0.00222	0.00000	-0.00035
S_0	S_2 MLCT(NHC)	2871	-0.01159	0.47582	0.17412	0.051667
S_0	Total dipole of TLC			-0.00989	0.00157	0.00126

Table S35. Energy differences in **2a**.

States @ opt geo	T_1-S_2 @ S0	T_1-S_2 @ T_{LC}
ΔE [eV]	0.587	1.650

8.6. The trigonal formyl pyridine complex **3b**

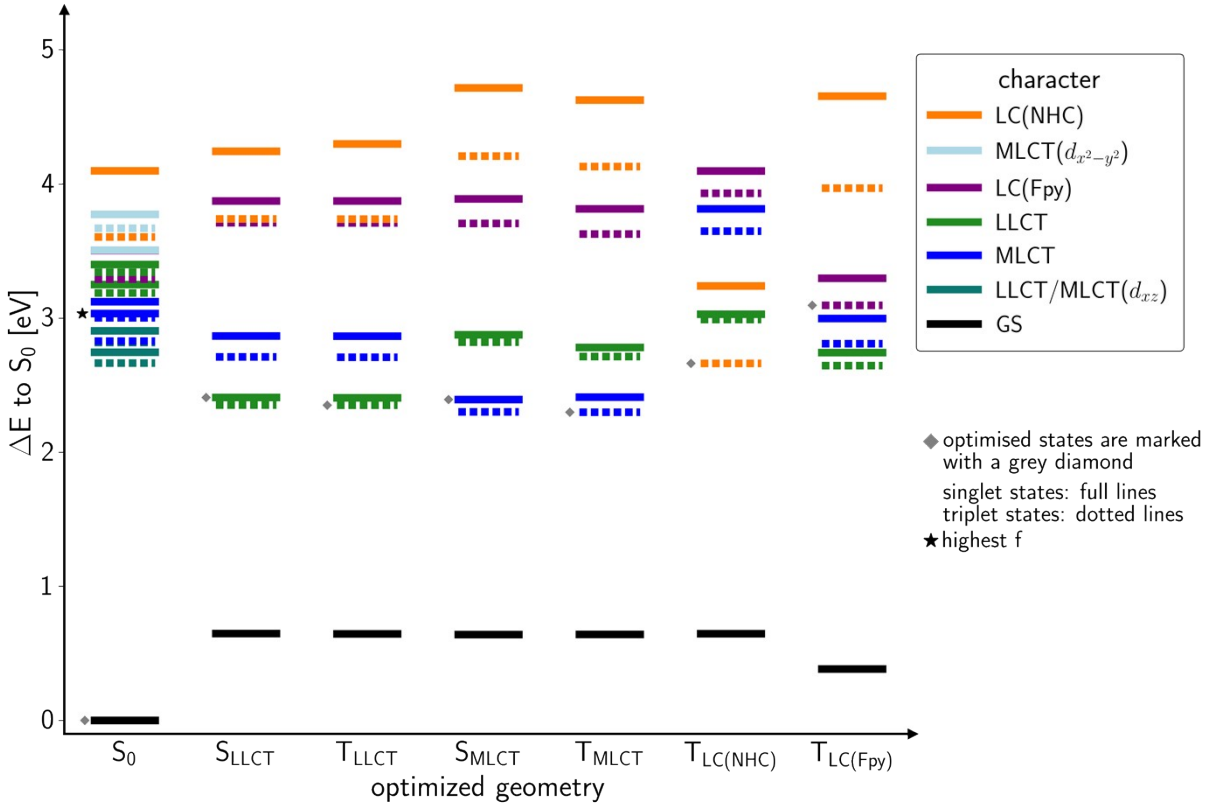

Figure S224. Energy state diagram of **3b** for selected optimized geometries.

Table S36. Singlet states and their properties at the ground state geometry of **3b**.

State	E [eV]	λ_{abs} [nm]	f	|μ| [D]	Character
S0	0			18.94	S0
S1	2.745	452	0.01507	3.87	LLCT/MLCT(xz)
S2	2.905	427	0.00305	-1.30	LLCT/MLCT(xz)
S3	3.034	409	0.13578	-10.02	MLCT
S4	3.122	397	0.07613	-11.11	MLCT
S5	3.250	381	0.01202	1.91	LLCT
S6	3.399	365	0.00421	4.44	LLCT
S7	3.504	354	0.00043	-10.09	LC(Fpy)
S8	3.508	353	0.00126	-11.15	LC(Fpy)
S9	3.774	329	0.04002	-3.19	MLCT(x2-y2)
S10	3.927	316	0.02047	16.57	MLCT(x2-y2)
S11	4.098	303	0.11954	9.59	LC(NHC)

Table S37. Triplet states and their properties at the ground state geometry of **3b**.

State	E [eV]			|μ| [D]	Character
T1	2.665			1.05	LLCT/MLCT(xz)
T2	2.818			2.61	LLCT/MLCT(xz)
T3	2.828			3.72	MLCT
T4	3.002			5.47	MLCT
T5	3.187			5.82	LLCT
T6	3.230			16.52	LC(Fpy)
T7	3.303			22.12	LC(Fpy)
T8	3.342			0.58	LLCT
T9	3.605			11.05	LC(NHC)
T10	3.670			6.24	MLCT(x2-y2)

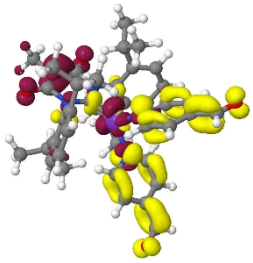

Figure S225. S1-S0 difference density at the GS of **3b**.

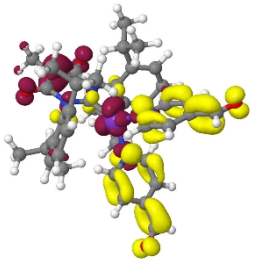

Figure S226. S2-S0 difference density at the GS of **3b**.

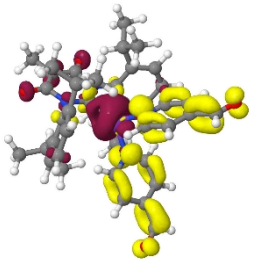

Figure S227. S3-S0 difference density at the GS of **3b**.

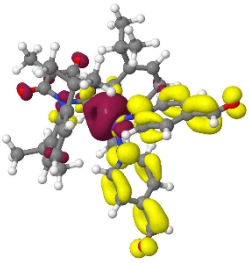

Figure S228. S4-S0 difference density at the GS of **3b**.

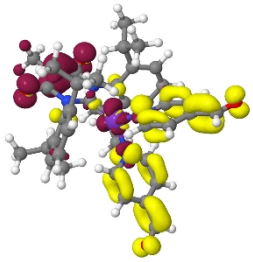

Figure S229. S5-S0 difference density at the GS of **3b**.

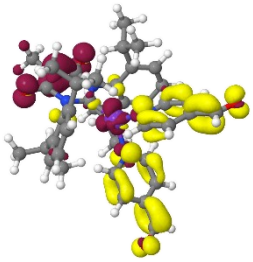

Figure S230. S6-S0 difference density at the GS of **3b**.

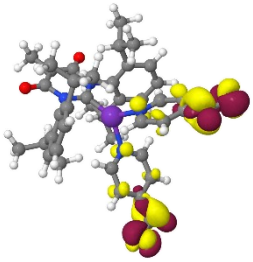

Figure S231. S7-S0 difference density at the GS of **3b**.

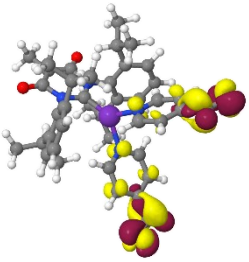

Figure S232. S8-S0 difference density at the GS of **3b**.

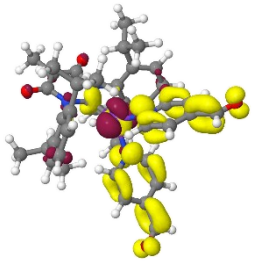

Figure S233. S9-S0 difference density at the GS of **3b**.

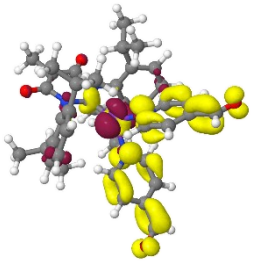

Figure S234. S10-S0 difference density at the GS of **3b**.

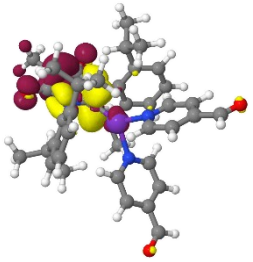

Figure S235. S11-S0 difference density at the GS of **3b**.

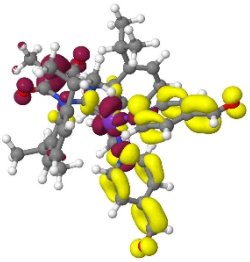

Figure S236. T1-S0 difference density at the GS of **3b**.

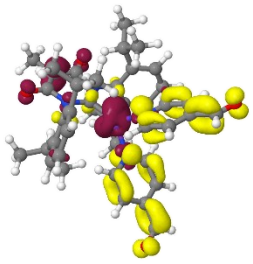

Figure S237. T2-S0 difference density at the GS of **3b**.

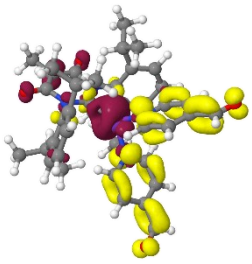

Figure S238. T3-S0 difference density at the GS of **3b**.

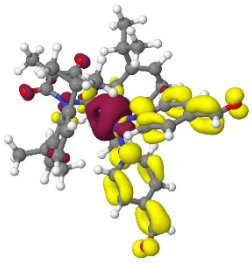

Figure S239. T4-S0 difference density at the GS of **3b**.

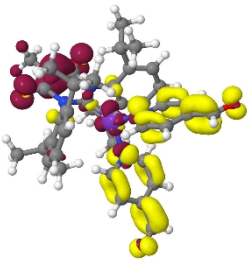

Figure S240. T5-S0 difference density at the GS of **3b**.

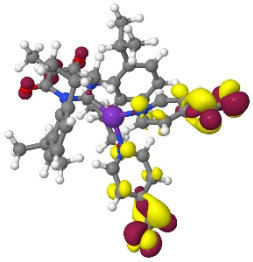

Figure S241. T6-S0 difference density at the GS of **3b**.

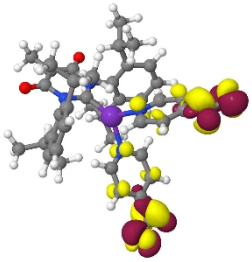

Figure S242. T7-S0 difference density at the GS of **3b**.

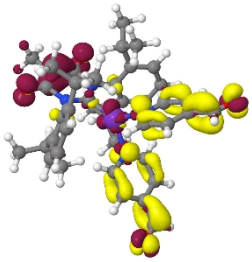

Figure S243. T8-S0 difference density at the GS of **3b**.

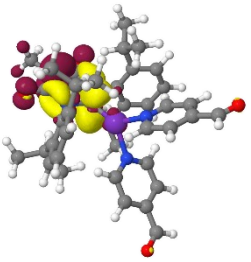

Figure S244. T9-S0 difference density at the GS of **3b**.

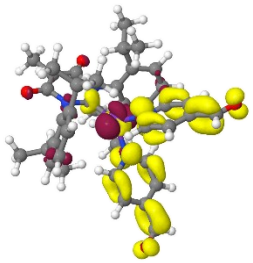

Figure S245. T10-S0 difference density at the GS of **3b**.

Table S38. Energies [eV] of relevant excited states of **3b** at the optimized geometries of different states.

State	Optimized geometry						
	S0	SLLCT	TLLCT	SMLCT	TMLCT	TLC(NHC)	TLC(Fpy)
S0	0.000	0.648	0.646	0.640	0.642	0.647	0.383
SLLCT	2.745	2.408	2.406	2.875	2.782	3.029	2.742
TLLCT	2.665	2.352	2.350	2.820	2.714	2.990	2.645
SMLCT	3.034	2.866	2.865	2.393	2.411	3.815	2.997
TMLCT	2.828	2.711	2.708	2.301	2.299	3.649	2.809
TLC(NHC)	3.342	3.739	3.738	4.208	4.130	2.663	3.968
TLC(Fpy)	3.303	2.711	3.710	3.706	3.627	3.931	3.095

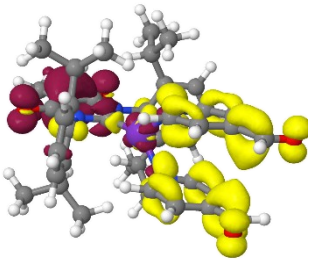

Figure S246. S1-S0 (LLCT) difference density at the **3b** SLLCT geometry.

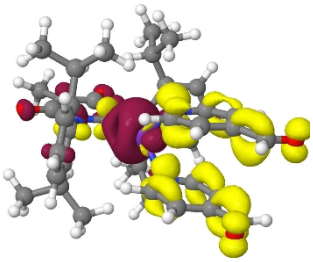

Figure S247. S1-S0 (MLCT) difference density at the **3b** SLLCT geometry.

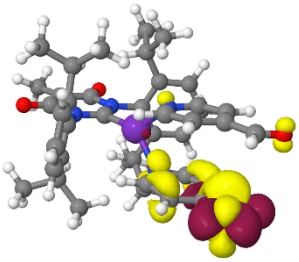

Figure S248. S7-S0 (LC(FLut)) difference density at the **3b** SLLCT geometry.

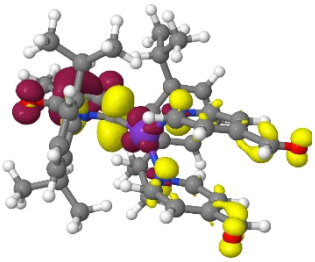

Figure S249. S12-S0 (LC(NHC)) difference density at the **3b** SLLCT geometry.

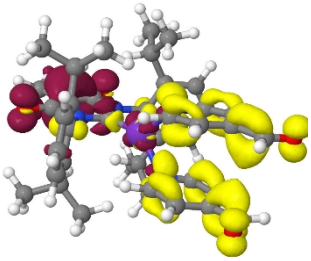

Figure S250. T1-S0 (LLCT) difference density at the **3b** SLLCT geometry.

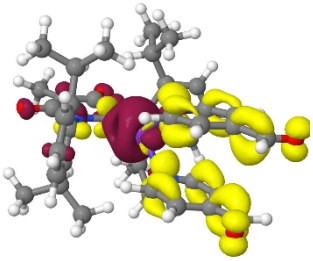

Figure S251. T2-S0 (MLCT) difference density at the **3b** SLLCT geometry.

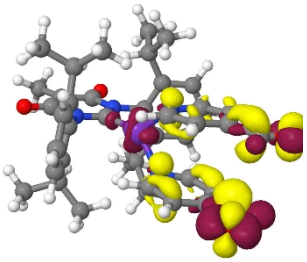

Figure S252. T7-S0 (LC(FLut)) difference density at the **3b** SLLCT geometry.

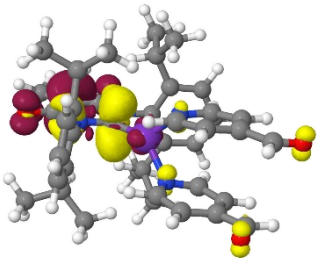

Figure S253. T9-S0 (LC(NHC)) difference density at the **3b** SLLCT geometry.

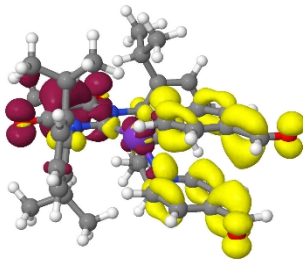

Figure S254. S1-S0 (LLCT) difference density at the **3b** TLLCT geometry.

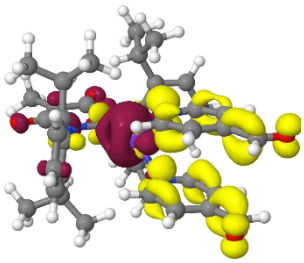

Figure S255. S2-S0 (MLCT) difference density at the **3b** TLLCT geometry.

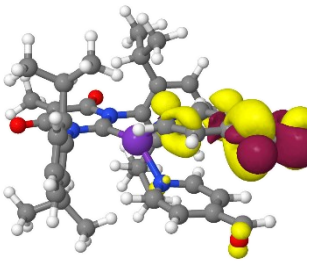

Figure S256. S7-S0 (LC(FLut)) difference density at the **3b** TLLCT geometry.

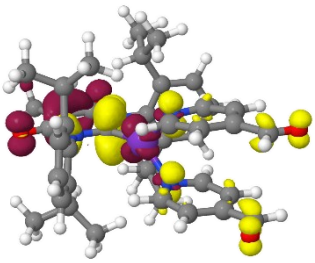

Figure S257. S1-S14 (LC(NHC)) difference density at the **3b** TLLCT geometry.

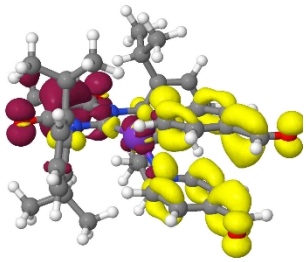

Figure S258. T1-S0 (LLCT) difference density at the **3b** TLLCT geometry.

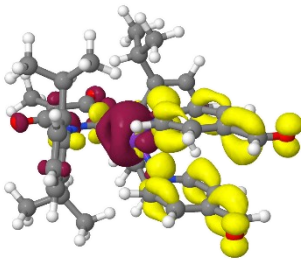

Figure S259. T2-S0 (MLCT) difference density at the **3b** TLLCT geometry.

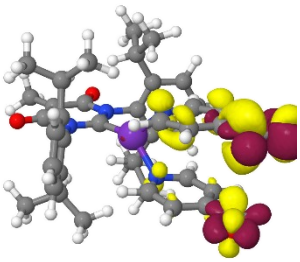

Figure S260. T7-S0 (LC(FLut)) difference density at the **3b** TLLCT geometry.

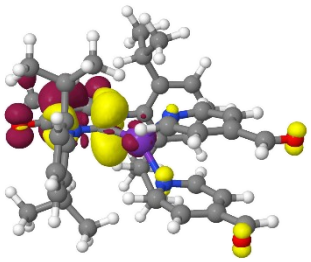

Figure S261. T9-S0 (LC(NHC)) difference density at the **3b** TLLCT geometry.

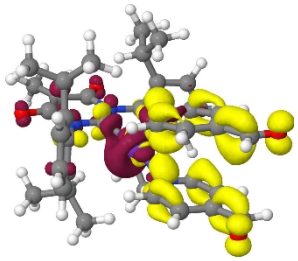

Figure S262. S1-S0 (MLCT) difference density at the **3b** SMLCT geometry.

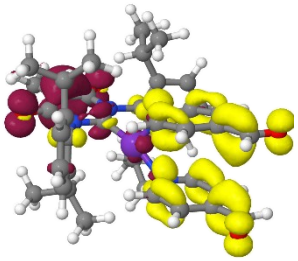

Figure S263. S1-S0 (LLCT) difference density at the **3b** SMLCT geometry.

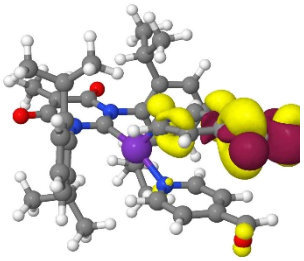

Figure S264. S7-S0 (LC(FLut)) difference density at the **3b** SMLCT geometry.

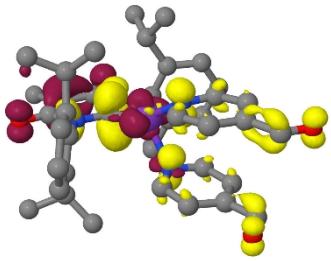

Figure S265. S20-S0 (LC(NHC) difference density at the **3b** SMLCT geometry.

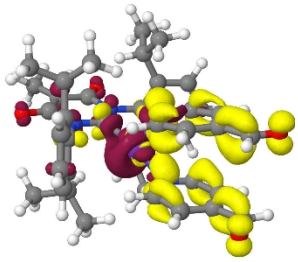

Figure S266. T1-S0 (MLCT) difference density at the **3b** SMLCT geometry.

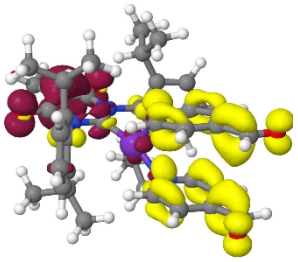

Figure S267. T2-S0 (LLCT) difference density at the **3b** SMLCT geometry.

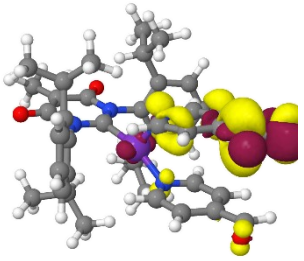

Figure S268. T6-S0 (LC(FLut)) difference density at the **3b** SMLCT geometry.

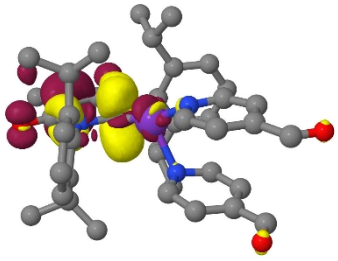

Figure S269. T14-S0 (LC(NHC)) difference density at the **3b** SMLCT geometry.

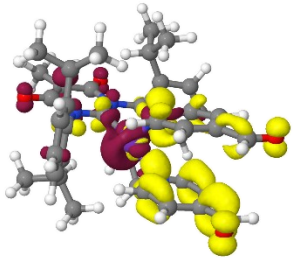

Figure S270. S1-S0 (MLCT) difference density at the **3b** TMLCT geometry.

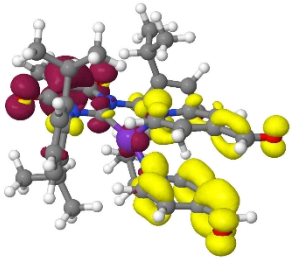

Figure S271. S2-S0 (LLCT) difference density at the **3b** TMLCT geometry.

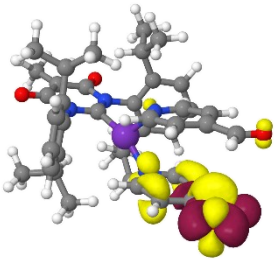

Figure S272. S7-S0 (LC(FLut)) difference density at the **3b** TMLCT geometry.

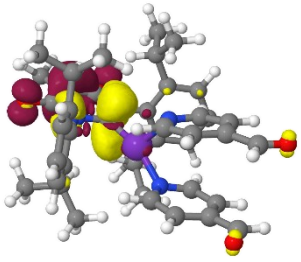

Figure S273. S19-S0 (LC(NHC)) difference density at the **3b** TMLCT geometry.

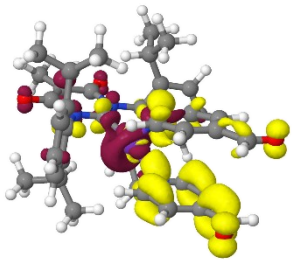

Figure S274. T1-S0 (MLCT) difference density at the **3b** TMLCT geometry.

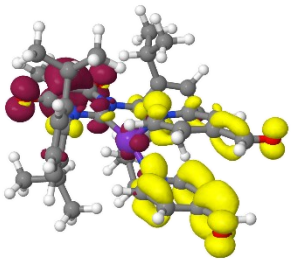

Figure S275. T2-S0 (LLCT) difference density at the **3b** TMLCT geometry.

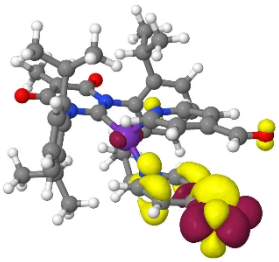

Figure S276. T6-S0 (LC(FLut)) difference density at the **3b** TMLCT geometry.

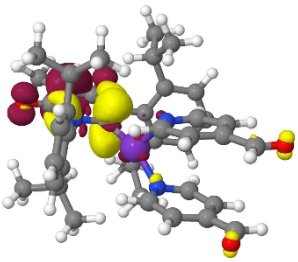

Figure S277. T14-S0 (LC(NHC)) difference density at the **3b** TMLCT geometry.

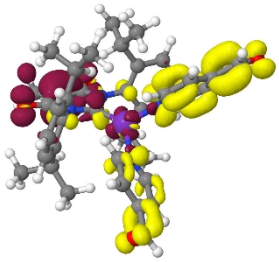

Figure S278. S1-S0 (LLCT) difference density at the **3b** TLC(NHC) geometry.

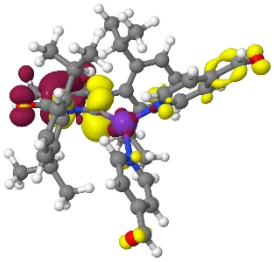

Figure S279. S3-S0 (LC(NHC)) difference density at the **3b** TLC(NHC) geometry.

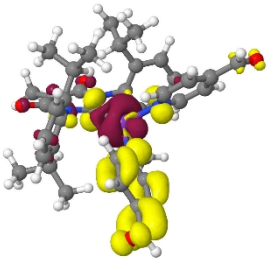

Figure S280. S6-S0 (MLCT(NHC)) difference density at the **3b** TLC(NHC) geometry.

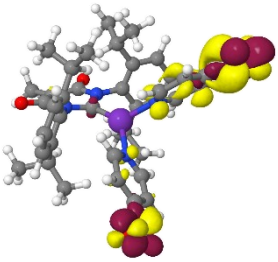

Figure S281. S8-S0 (LC(FLut)) difference density at the **3b** TLC(NHC) geometry.

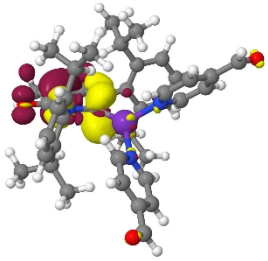

Figure S282. T1-S0 (LC(NHC)) difference density at the **3b** TLC(NHC) geometry.

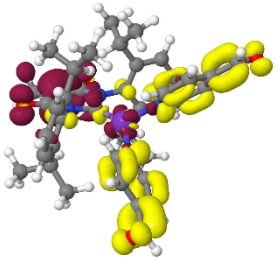

Figure S283. T2-S0 (LLCT) difference density at the **3b** TLC(NHC) geometry.

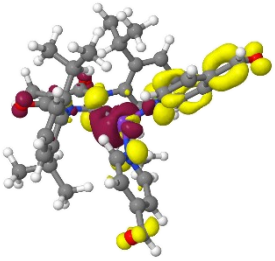

Figure S284. T5-S0 (MLCT) difference density at the **3b** TLC(NHC) geometry.

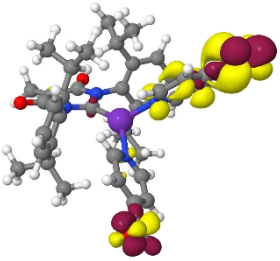

Figure S285. T9-S0 (LC(FLut)) difference density at the **3b** TLC(NHC) geometry.

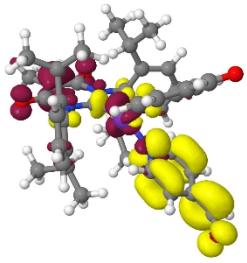

Figure S286. S1-S0 (LC(FLut)) difference density at the **3b** TLC(Fpy) geometry.

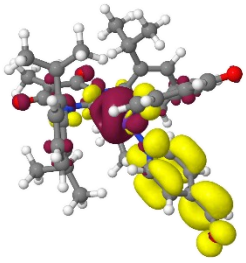

Figure S287. S2-S0 (LC(FLut)) difference density at the **3b** TLC(Fpy) geometry.

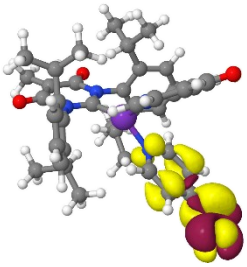

Figure S288. S5-S0 (LC(FLut)) difference density at the **3b** TLC(Fpy) geometry.

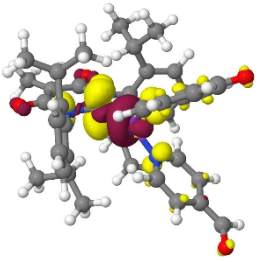

Figure S289. S17-S0 (LC(FLut)) difference density at the **3b** TLC(Fpy) geometry.

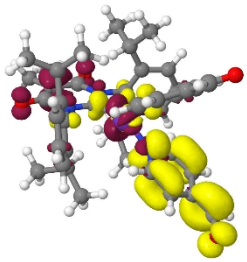

Figure S290. T1-S0 (LC(FLut)) difference density at the **3b** TLC(Fpy) geometry.

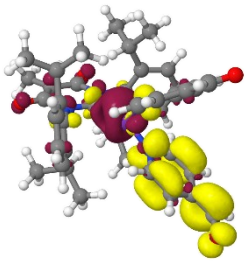

Figure S291. T2-S0 (LC(FLut)) difference density at the **3b** TLC(Fpy) geometry.

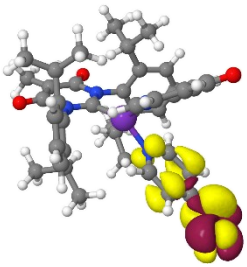

Figure S292. T3-S0 (LC(FLut)) difference density at the **3b** TLC(Fpy) geometry.

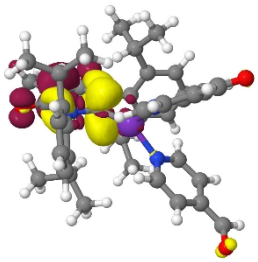

Figure S293. T11-S0 (LC(FLut)) difference density at the **3b** TLC(Fpy) geometry.